Frontiers of Astronomy, Astrophysics and Cosmology, 2015, Vol. 1, No. 1, 56-73
Available online at http://pubs.sciepub.com/faac/1/1/7
© Science and Education Publishing
DOI:10.12691/faac-1-1-7

The Action of Water Vapor on the Stratospheric Ozone Chemistry

Yasuaki Ito, Akiyoshi Matsuzaki*

Faculty of Engineering, Mie University, Kurimamachiyamachi 1577, Tsu, Mie 514-8507, Japan
*Corresponding author: matuzaki@ chem.mie-u.ac.jp

Received December 31, 2014; Revised February 22, 2015; Accepted June 26, 2015

Abstract The action of water vapor on the stratospheric ozone chemistry is studied in the low latitude region and the Polar Regions with the data of the solar-occultation infrared spectrometers LAS boarding the satellite OHZORA (EXOS-C) and ILAS boarding the satellite Midori (ADEOS), respectively. The study in the low latitude region with the LAS data on 4 April 1984 indicates the clear anti-correlation between the water vapor and ozone concentrations at the altitudes of 30 and 40 km, where the ultraviolet-photochemical reactions are very active, and the less clear one at 20 and 10 km, where they are rather inactive. Furthermore the longitudinal distribution of the stratospheric ozone suggests that it is affected by the interaction between the up-stream of water vapor and the tropospheric northern wind in the present case. These facts are discussed by the ozone chemistry with the HO_x catalytic chemistry. On the other hand, the present study on the stratospheric ozone chemistry in the Polar Regions with use of the ILAS data also finds the evident anti-correlation between the water vapor and ozone concentrations, as well as the evident altitude dependence of the stratospheric ozone chemistry and an evident difference in the stratospheric chemistry inside and outside Ozone Holes. These facts are discussed by the ozone chemistry with the HO_x catalytic chemistry and the ozone chemistry with the polar stratospheric clouds, which includes the HO_x, NO_x, and ClO_x catalytic chemistry. Furthermore, we try to add the total ozone longitudinal circular maps in the regions, where NASA's TOMS total ozone maps are unavailable in the winter seasons in the Polar Regions, by using the ILAS data observed on the boundaries between the day and night sides. As a result, we succeed in providing the NASA's TOMS maps with the total column ozone circular maps by the ILAS data.

Keywords: *stratospheric ozone, water vapor, Ozone Hole, LAS, ILAS, ILAS-II*

Cite This Article: Yasuaki Ito, and Akiyoshi Matsuzaki, "The Action of Water Vapor on the Stratospheric Ozone Chemistry." *Frontiers of Astronomy, Astrophysics and Cosmology*, vol. 1, no. 1 (2015): 56-73. doi: 10.12691/faac-1-1-7.

1. Introduction

The stratospheric ozone chemistry is essentially represented by Chapman's model [1]. Yet, to represent the real atmosphere better, the model has been modified by adding the chemical processes known as HO_x, NO_x, and ClO_x cycles [2,3,4]. The NO_x cycle was regarded as the predominant process in the contribution of these cycles to the Chapman model, since N_2 is the major constituent and H_2O and halogen compounds are the minor constituents in the atmosphere [5]. Nevertheless, the Stratospheric Photochemistry Aerosols and Dynamics Expedition (SPADE) in 1993 and the Airborne Southern Hemisphere Ozone Experiment (ASHOE) in 1994 gave the significantly interesting results [6]: in the region between 15˚ and 60˚ Northern latitude at altitude up to 21 km, the HO_x cycle is the predominant mechanism, accounting for approximately 50 % of the ozone removal rate, and the ClO_x cycle accounts for approximately 33 % of it and the NO_x cycle does for approximately 17 % of it [5]. Under the circumstances, it is of great interest to study the action of water vapor on the stratospheric ozone chemistry from the global viewpoints.

Recent development in techniques of atmospheric remote sensing from satellites provides us the high quality atmospheric data, as well as those from balloon and other in-situ experiments. For instance, the SAGE series consisting of SAM I/II in 1975/78, SAGE I in 1975, SAGE II in 1984, SAGE III Meteor-3M in 2001, and SAGE III ISS in 2016 is a typical significant one [7]. We developed the infrared spectrometers called LAS, ILAS, and ILAS-II for the experiments with the satellites called OHZORA, ADEOS, and ADEOS-II, respectively [8,9,10]. These spectrometers measure the infrared spectra at the times of sunset and sunrise for the satellite by a solar occultation method and hence, provide the good height profiles of the atmospheric constituent concentrations, as SAGE does. The spectrometers measure the whole bands of atmospheric constituents by multichannel spectroscopy with use of pyroelectric linear arrays and CCD/photodiode linear arrays. The validation through the balloon and other in-situ and remote sensing experiments has been made for ILAS and ILAS-II and reported the high quality of the data [11,12]. In the present paper, we study the action of water vapor on the stratospheric chemistry in the low-

latitude region and the Polar Regions with use of the LAS and ILAS data, respectively.

2. Experimental

2.1. LAS

LAS (Limb atmospheric infrared spectrometer) was developed for the satellite OHZORA (EXOS-C) of ISAS (the Institute of Space and Astronautical Science) in Japan [13, 14]. It was launched into the semi-polar orbit in February 1984. Its heights at the perigee and the apogee were 354 and 865 km, respectively, the inclination was 74.6˚, and the period was 97 min on 4 April 1984. The photographs of LAS and OHZORA are shown in Figure 1a and b, respectively. Figures 2a and b show the schematic illustration of the LAS optical system, which corresponds to the optical system in Figure 1a, and the schematic diagram of the LAS optical system, respectively.

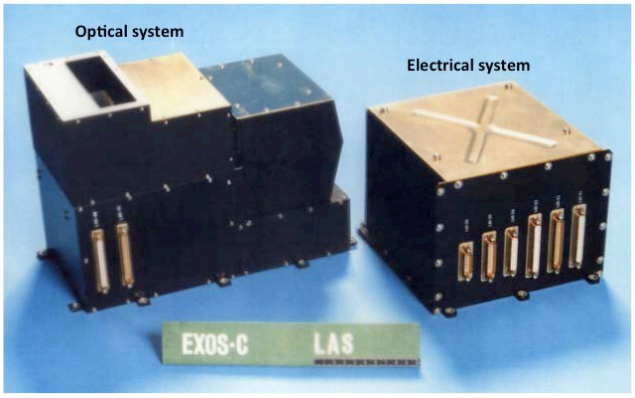

Figure 1a. LAS (Limb atmospheric infrared spectrometer)

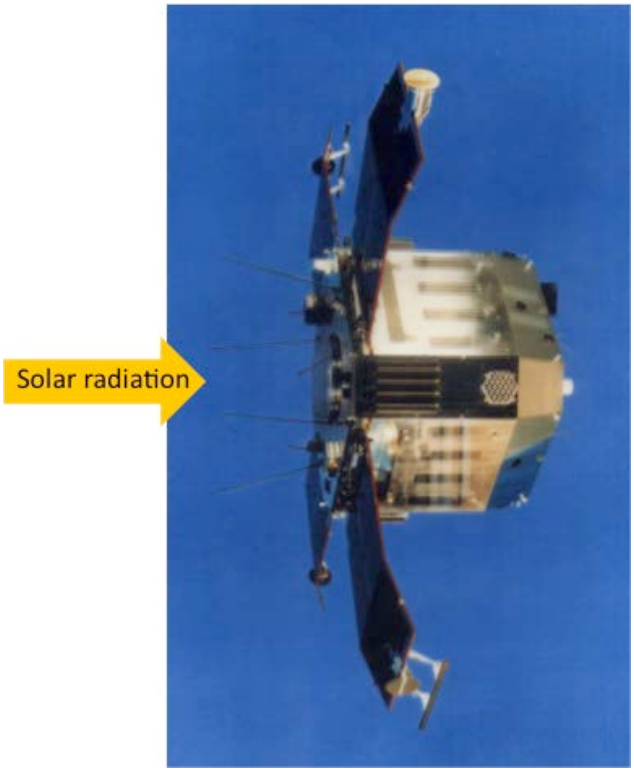

Figure 1b. Satellite OHZORA (EXOS-C)

As schematically shown in Figures 2a and b, LAS measures the infrared spectra in three wavelength regions. The specs of LAS in these wavelength ranges are shown in Table 1.

Table 1. The Specs of LAS in Three Wavelength Regions

Range	Wavelength/μm	Sensor	Constituents
1	1.6-2.4	32-elements $LiTaO_3$ linear array	H_2O, aerosol
2	2.8-4.8	64-elements $LiTaO_3$ linear array	CO_2, CH_4, N_2O, H_2O, aerosol
3	8.8-10.2	16-elements $PbTiO_3$ linear array	O_3

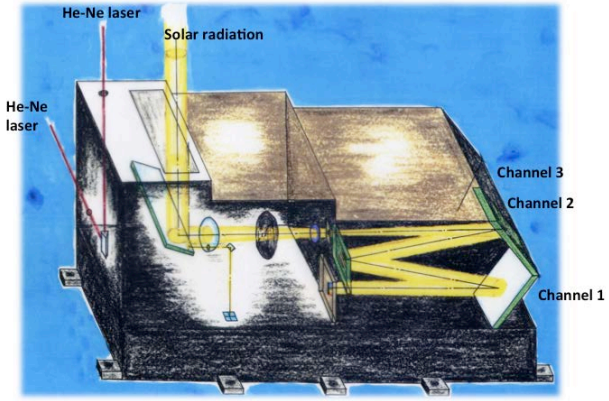

Figure 2a. Schematic illustration of LAS optical system, where only the optical path of Channel 1 is drawn. The He-Ne laser was introduced into LAS from the outside the satellite for the optical alignment before the launch

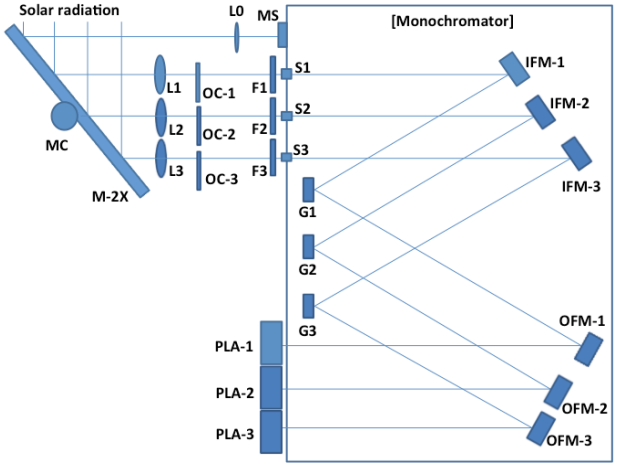

Figure 2b. Schematic diagram of LAS optical system. MC: two motors, M-2X: a two-axes controlled mirror, L1-L3: focus lenses, OC-1–OC-3: optical choppers, S1-S3: slits, IFM-1–IFM-3 and OFM-1–OFM-3: concave mirrors, G1–G-3: gratings, PLA-1–PLA-3: pyroelectric linear array sensors, L0: a focus lens, MS: a 2x2-matrix sensor

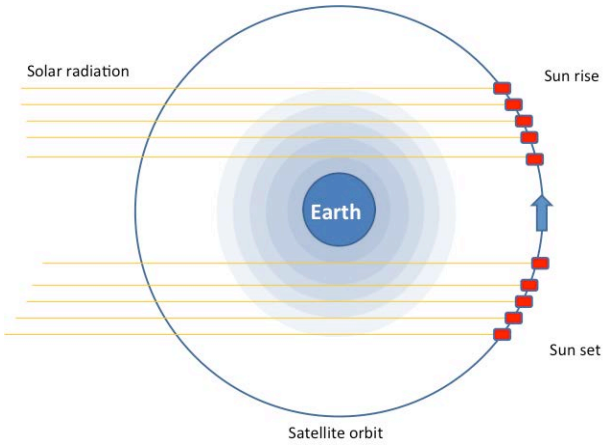

Figure 3. Observation by a solar occultation method

As the sensors of the SAGE series of NASA, LAS is a solar occultation sensor, as shown in Figure 3, measuring the infrared spectra of the solar radiation passing through the atmosphere at the tangential heights above the tangential points in the sunrise and sunset events. The solar occultation method has the advantage in the altitude distribution analysis of the atmospheric constituents.

The data obtained by the solar occultation method is usually analyzed by an onion peel method. For instance, the following equation is used for the ozone analysis.

$$B(O_3) = A(O_3)L \quad (1)$$

In Equation 1, $\boldsymbol{B}(O_3)$, $\boldsymbol{A}(O_3)$, and $\boldsymbol{L}$ are the vector of the ozone absorption intensity measured at the individual tangent heights, the vector of the ozone absorption intensity per km at the individual tangent heights, and the tensor, which is the triangle matrix, of the optical lengths of the solar radiation in the individual atmospheric layers at the individual tangent heights, respectively. Since $\boldsymbol{B}(O_3)$ and $\boldsymbol{L}$ are obtained from the satellite data and by the geometric calculation, respectively, $\boldsymbol{A}(O_3)$ can be determined by Equation 1. It is significant to note that the analysis can definitely proceed without any hypothetic estimation, giving the advantage in the altitude distribution analysis.

2.2. ILAS

ILAS (Improved limb atmospheric infrared spectrometer) was developed by the Environmental Agency of Japan for the satellite Midori (ADEOS) of NASDA (the National Space Development Agency of Japan). It was launched into the sun synchronous semi-recurrent orbit of an altitude approx. 830 km on 17 August in 1996. The schematic diagram of ILAS and the illustration of ADEOS are shown in Figure 4a and b, respectively.

ILAS consists of the infrared spectrometer and the visible spectrometer. The infrared spectrometer was developed from LAS, which is the reason for naming ILAS. The visible spectrometer is based on the spectrometer for the rocket experiments, which measured the rotational profiles of the atmospheric band of O_2 to observe the altitude profiles of the atmospheric temperature [15,16] and the balloon experiment [17]. The details of the ILAS system can be available in the references [9,18]. The specs of ILAS are shown in Table 2.

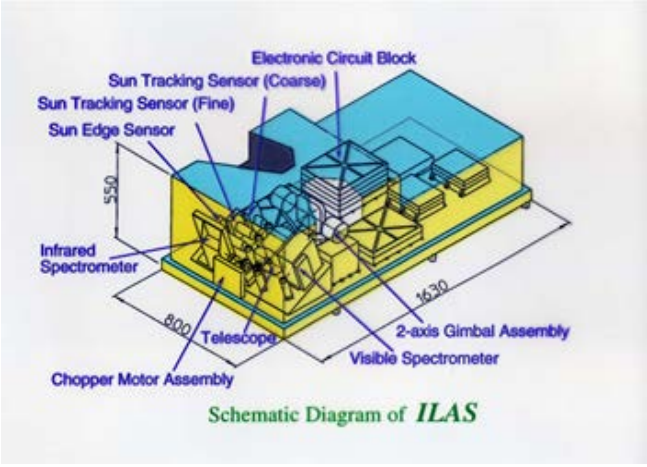

Figure 4a. ILAS (Improved limb atmospheric infrared spectrometer) with the sizes in mm

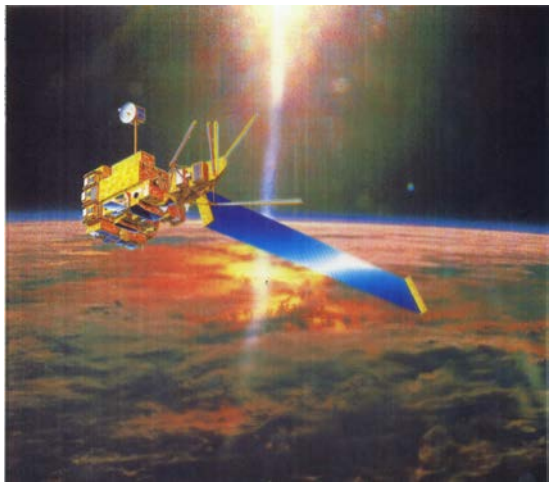

Figure 4b. Satellite Midori (ADEOS)

Table 2. Specs of ILAS

Grating spectrometers with linear array detectors	IR	44-pixels pyroelectric linear array
	Visible	1024-pixels MOS photodiode array
Spectral coverage / resolution	Coverage (IR)	850-1610 cm^{-1} (6.21-11.77 μm)
	Resolution (IR)	0.129 μm
	Coverage (VIS)	753-784 nm
	Resolution (VIS)	0.15 nm
IFOV (Vertical x horizontal)	IR	2 km x 13 km
	Visible	2 km x 2 km
Positioning	Tracking radiometric center of the sun from the cloud top up to 200 km	
	IFOV position measurement from the top edge of the sun with a resolution of 8 arc seconds with a 1024-pixels linear array detector	
Weight	130 kg	
Power	78 W	
Target species	O_3, NO_2, N_2O, N_2O_5, H_2O, HNO_3, CH_4, CO_2, CFC-11, CFC-12, aerosol	

The ILAS data analysis was made essentially by an onion peel method with Equation 1, as the LAS data analysis was. The details of the analysis are available in the references [9,11,18].

2.3. ILAS-II

The successful ILAS project was followed by ILAS-II, which was developed by the Environmental Agency of Japan for the satellite Midori-II (ADEOS-II) of NASDA (the National Space Development Agency of Japan). It was launched into the sun synchronous semi-recurrent orbit of an altitude approx. 802.9 km with the inclination of 98.62˚ on 14 December in 2002 [19]. The ILAS-II has almost the same instruments as ILAS [10, 12]. In the present study, we do not use the ILAS-II data.

2.4. Characteristics of LAS, ILAS, and ILAS-II

The following is a summary of the characteristics of LAS, ILAS, and ILAS-II as the satellite sensors:

1. They are the infrared spectrometers, since many atmospheric species have the absorption bands in the infrared region.
2. They are the solar occultation, i.e., the SAGE-type, spectrometers, giving the data with the high altitude resolution.

3. They measure the whole spectra of the constituents over the wavelength regions, greatly increasing the quality of the data analysis.
4. They have no cooling system in spite of the fact that they are the infrared spectrometers.

These characteristics are due to the use of multichannel spectroscopy with pyroelectric array sensors, which enables the quick wavelength sweeping [20,21]. Since the pyroelectric sensors detect only the thermal change, they can avoid the ambient thermal interference.

3. Results and Discussion

In Section 3.1, we will study the action of water vapor on the stratospheric ozone chemistry in the low latitude region in spring by the analysis of the LAS data. In Section 3.2, we will study the action of water vapor on the stratospheric ozone chemistry in the Polar Regions by the analysis of the ILAS data. In Section 3.3, we will make the total column ozone maps in the Polar Regions by the analysis of the ILAS data, providing the NASA's TOMS maps with the total column ozone map circles by the ILAS data, since there are the regions, where NASA's TOMS total ozone maps are unavailable in the winter seasons in the Polar Regions.

3.1. Action of Water Vapor on Stratospheric Ozone Chemistry in Low Latitude Region

The infrared spectra in regions of 1.6-2.4 and 8.8-10.2 μm, which were measured in the first and third channels of LAS, are shown in Figure 5 and Figure 6, respectively. As shown in Figure 5, the absorption band of ozone is observed in the infrared spectrum in region of 8.8-10.2 μm, indicating that the ozone spectrum observed with LAS agrees well with the theoretical spectrum. Besides, we can clearly confirm the absorption bands of water vapor in the infrared spectra in region of 1.6-2.4 μm, as shown in Figure 6.

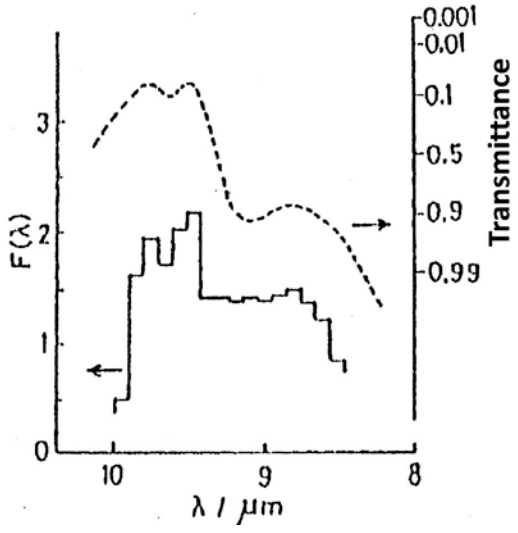

Figure 5. Spectrum measured in the third channel of LAS (solid line) and the theoretical spectrum of ozone [22] (dashed line). F(λ) is absorbance

Thus, since it is found that LAS measured the reliable spectra of ozone and water vapor in channels 3 and 1, respectively, we study the stratospheric ozone chemistry by using the LAS ozone and water vapor spectral data measured at 4˚N of latitude on 6 April in 1984, i.e., from 07:43 UT on 6 April to 01:30 UT on 7 April in 1984. As shown in Figure 7, the LAS observation was made in orbits 733, 734, 776-781, and 784, indicating the observation points, i.e. the tangential points, between 0 and 100 km of tangential heights by the solid lines. These observation points are on the day-night boundary, since LAS is the solar-occultation spectrometer. Hence the data of LAS includes the information of both the day and night sides. This fact will be significant for the discussion on the photo-chemically unstable species.

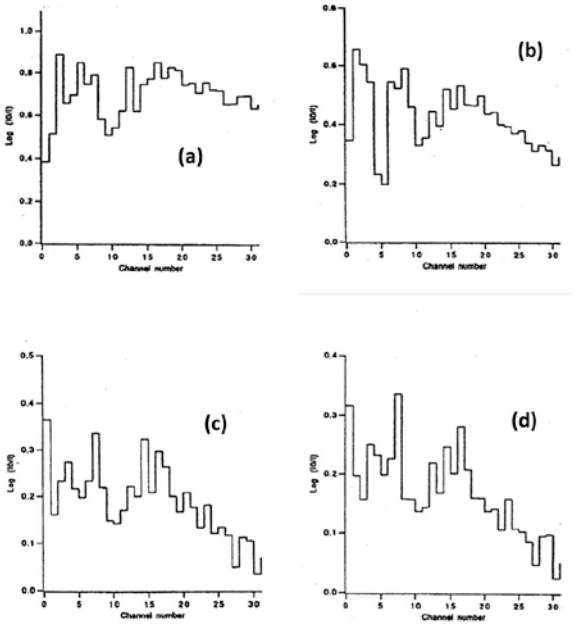

Figure 6. Spectra measured in the first channel of LAS; (a) 10 km, (b) 20 km, (c) 30 km, (d) 40 km of tangential heights, where wavelengths are 1.6 μm at channel number 0 and 2.4 μm at channel number 32 in the abscissa. Ordinate indicates the absorbance of the spectra

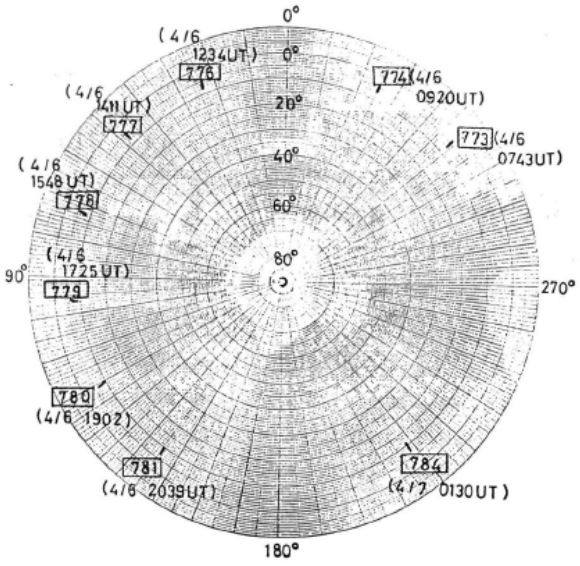

Figure 7. LAS observation points (tangential points) between 0 and 100 km of tangential heights in orbits 773-784 from 07:43 UT on 6 April to 01:30 UT on 7 April in 1984

By using the spectral data at these observation points, we obtain the longitudinal distribution of the absorption intensity of ozone and water vapor at the altitudes of 10, 20, 30, and 40 km at 4˚N of latitude on 6-7 April in 1984,

as shown in Figure 8 and Figure 9, respectively. Figure 8 indicates that the ozone population at 40 km is very high at orbit 779 and very low at its both sides, i.e. orbits 778 and 780. The figure also shows that this feature is evident at 30 km, i.e., the ozone population is very high at orbits 778 and 779 and very low at its both sides, i.e., orbits 777 and 780. This characteristic feature is most clear at 40 km and becomes weak with a decrease in the altitude. On the other hand, Figure 8 indicates that the water vapor population at 40 km is very high at orbit 778 and very low at its both sides, i.e. orbits 776, 777, 779, and 780. The figure also shows that this feature is evident at 30 km, i.e., the water vapor population is very high at orbits 777 and 778 and very low at its both sides, i.e., orbits 776 and 779. This characteristic feature is very clear at 30 and 40 km, clear at 20 km, and becomes weak at 10 km.

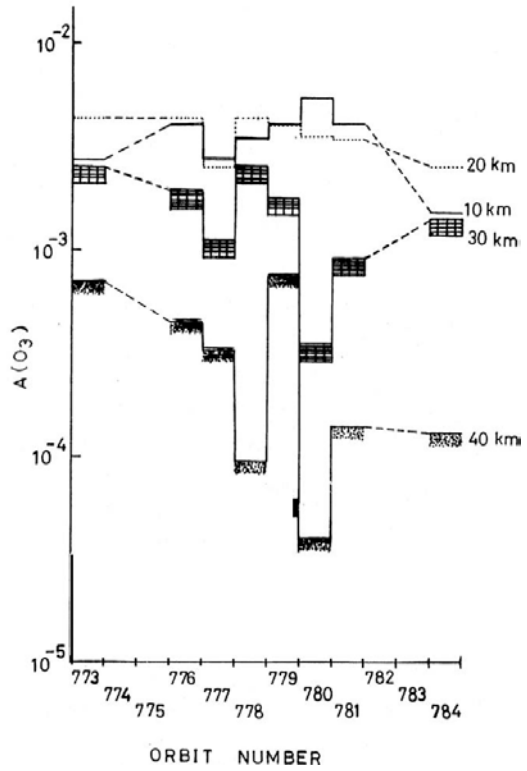

Figure 8. Ozone absorption intensity per km, i.e. A(O_3) in Equation 1, at various orbits

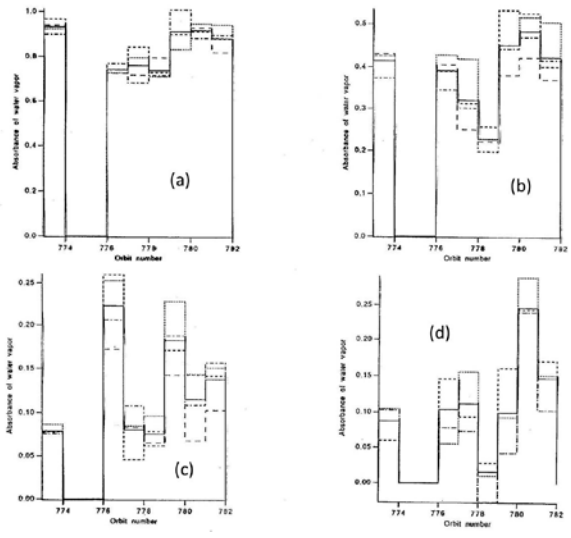

Figure 9. Water vapor absorption intensity at various orbits; (a) 10 km, (b) 20 km, (c) 30 km, (d) 40 km of altitude

The comparison between the characteristic features in the longitudinal distribution of ozone and water vapor in Figure 8 and Figure 9, respectively, suggests the inverse correlation between ozone and water vapor populations at 30 and 40 km of altitude. In fact, for instance, the correlation of the absorption intensity between ozone and water vapor at 30 km indicates the evident anti-correlation, as shown in Figure 10. The same plot has been made at 10, 20, and 40 km and the anti-correlation is found to be strong at 30 and 40 km and to decrease with a decrease in altitude, which exactly corresponds to the results in Figure 8 and Figure 9. Thus, these results indicate that water vapor reduces the ozone density at higher altitudes, where the ultraviolet solar radiation is strong, suggesting that the photochemical reactions between water vapor and ozone through the ultraviolet solar radiation decrease the ozone density at 30 and 40 km at the low northern latitudes in spring.

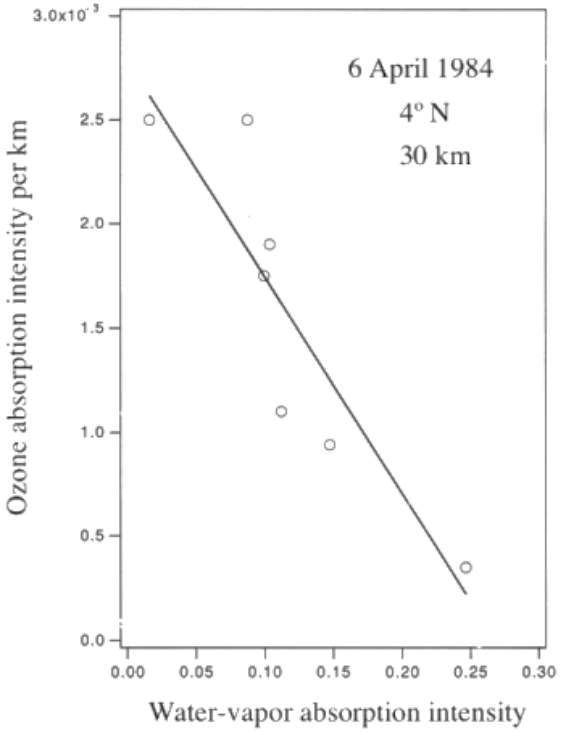

Figure 10. Plot of ozone absorption intensity per km, i.e. A(O_3), as a function of water-vapor absorption intensity at 30 km of altitude

Then, let us study the characteristic features in Figure 8 and Figure 9 that the ozone density is minimum on the both sides of the region, where the ozone density is maximum, and that the water vapor density is maximum on the both sides of the region of the minimum water-vapor density. For the study, we made the plot in Figure 11.

Figure 11 shows the positions of the northern wind in the troposphere, which were assigned by using the meteorological data from the Meteorological Agency of Japan, the regions of maximum and minimum water-vapor concentrations on the wind, which were also assigned by the same meteorological data from MAJ, and the regions of the maximum ozone concentrations at 20, 30, and 40 km, which are due to the present LAS data. While there are the regions of the minimum ozone concentrations on the both sides of the regions of the maximum ozone concentrations at 20, 30, and 40 km, notice that the regions of the minimum ozone concentrations are not

shown in Figure 11. As a result, we can find that Figure 11 indicates that all these regions, i.e., the positions of the northern wind in the troposphere, the positions of the maximum and minimum water vapor in the troposphere, and the positions of the maximum ozone concentrations in the stratosphere, can be connected as a smooth stream.

Thus, the present significant facts in Figure 11 strongly suggest that we have to discuss the mechanism for the characteristic features of ozone and water vapor distribution in Figure 8 and Figure 9 by taking account of the interactions between the upward stream of water vapor and the northern wind in the troposphere and the photochemical reactions between ozone and water vapor through the ultraviolet solar radiation in the stratosphere. On the basis of these guidelines, we consequently deduce the model in Figure 12.

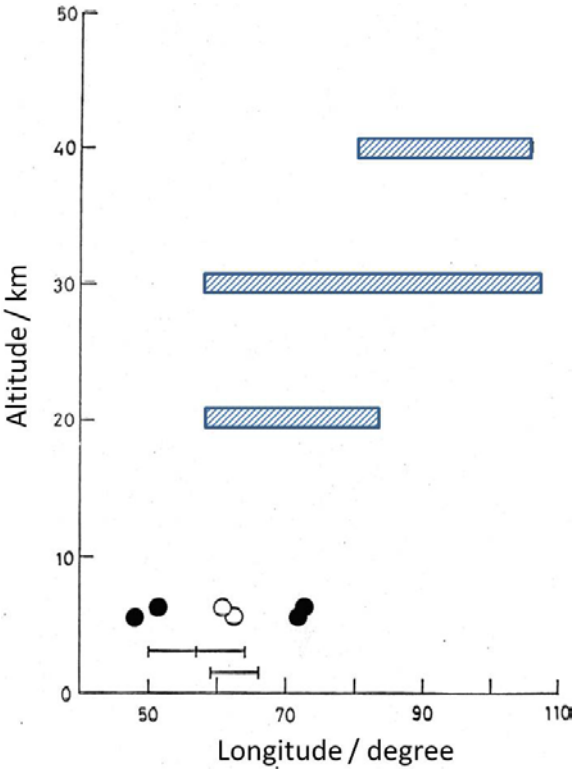

Figure 11. The solid horizontal bars indicate the positions of the northern wind, the solid circles and the open circles indicate the positions of the maximum and minimum concentrations of water vapor, respectively, and the striped horizontal bars indicate the positions of the maximum ozone concentrations at 20, 30, and 40 km of altitudes

As shown in Figure 12, the interaction between the upward stream and the northern wind results in the inhomogeneous distribution of water vapor. This will be due to the mechanism that the water vapor concentration is low on the wind and high on its both sides through a kind of the slip-stream effect. That is, the upstream is disturbed at the northern wind and rather rapidly passes on the both sides of the wind. The water vapor distribution by this mechanism turns out to be in agreement with the one in Figure 11. When the tropospheric atmosphere with this inhomogeneous water-vapor distribution is input into the stratosphere, the inhomogeneous ozone distribution will be formed through the photochemical reactions between ozone and water vapor, as shown in Figure 12, since the reactions reduce the ozone concentration. Thus it is found that the ozone and water vapor distribution deduced by the mechanism in Figure 12 agrees well with the characteristic features of the ozone and water vapor distribution in Figure 8 and Figure 9, respectively, deduced from the experimental data.

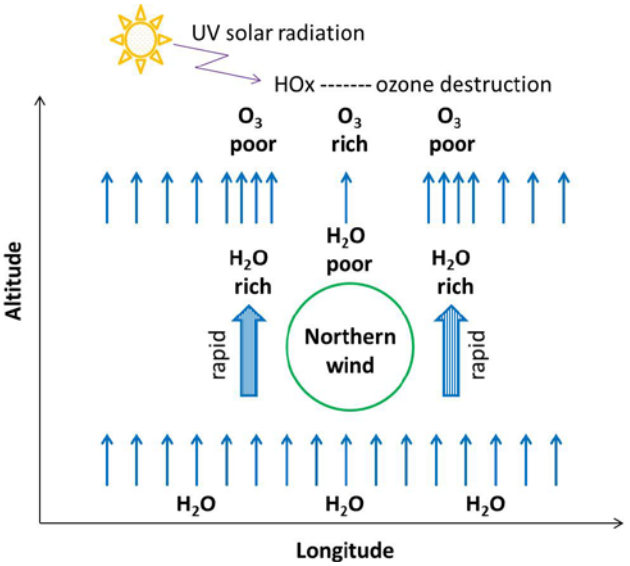

Figure 12. Schematic illustration for understanding the characteristic features of ozone and water vapor distribution observed at 4˚N of latitude on 6 April in 1984

Since we find that the mechanism in Figure 12 agrees well with the experimental facts in Figure 8-Figure 11, let us validate the two guidelines in the mechanism in Figure 12. First, the presence of the upward stream will be real, since we remember that ITCZ (Intertropical Convergence Zone) is placed in the present low-latitude region, i.e. at 4˚N of latitude, in spring, i.e., in April. Thus, the tropospheric atmosphere is input into the stratosphere by the upward stream through ITCZ. Furthermore the presence of the northern wind is real, too, since it was confirmed with the meteorological data, as described above. Therefore, the first guideline has been confirmed to be appropriate. On the other hand, as mentioned in the introduction section of this paper, the SPADE and ASHORE results [6] will strongly suggest the appropriateness of the second guideline that the photochemical reactions between ozone and water vapor through the ultraviolet radiation will reduce the stratospheric ozone concentration.

In fact, for the altitude less than 50 km, the following scheme, Scheme 1, is proposed for the photochemical catalytic reaction with HO_x [2,5,23]:

Scheme 1:

$$O_3 + hn \rightarrow O\left(^1D\right) + O_2 \quad \text{Photodissociation of ozone} \quad (2)$$

$$H_2O + O\left(^1D\right) \rightarrow 2OH \quad \text{OH formation from } H_2O \quad (3)$$

$$OH + O_3 \rightarrow HO_2 + O_2 \quad \text{Ozone extinction by OH} \quad (4)$$

$$HO_2 + O_3 \rightarrow OH + 2O_2 \quad \text{Ozone extinction by } HO_2 \quad (5)$$

$$OH + HO_2 \rightarrow H_2O + O_2 \quad \text{Reproduction of } H_2O \quad (6)$$

Through the scheme, the ozone concentration is reduced, while the H_2O concentration is invariable. The solar radiation concerns the scheme by photo-dissociating ozone in Process (2). Thus, based on the above discussion, here we conclude that the second guideline of the mechanism in Figure 12 is also appropriate. In conclusion,

through the study in this section, we can find the situation similar to the one of SPADE and ASHORE for the action of water vapors on the stratospheric ozone chemistry in the low latitude region in spring.

3.2. Action of Water Vapor on Stratospheric Ozone Chemistry in Polar Regions

In this section, we study the action of water vapor on the stratospheric ozone chemistry in the Polar Regions by the analysis of the ILAS data.

3.2.1. Altitude-Longitude Maps of Ozone and Water Vapor

Figure 13 shows the altitude-longitude maps of water vapor and ozone in the Antarctic region on 17 November in 1996, which are made by the ILAS data analysis. The comparison between the water-vapor map on the left panel and the ozone map on the right panel indicates that the ozone concentration is high in the regions where the water-vapor concentration is low; i.e., the anti-correlation between the ozone and water vapor concentrations is confirmed also in this case. The careful comparison between the H_2O and O_3 maps evidently indicates the anti-correlation between the water vapor and ozone distribution at the altitudes of 20-45 km.

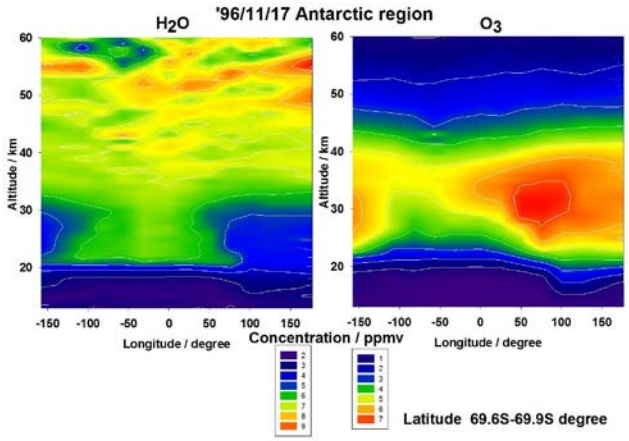

Figure 13. The ILAS data showing the altitude-longitude maps of water vapor and ozone in the Antarctic region on 17 November in 1996

3.2.2. Seasonal Variations in Ozone and Water Vapor Concentrations

Figure 14 shows the seasonal variations in the ozone and water-vapor concentrations of the ozone layer outside the Ozone Hole in the Antarctic region, which are made by the ILAS data analysis. The comparison between the variations in the water-vapor concentration on the bottom panel and the ozone concentration on the top panel indicates the evident anti-correlation.

On the other hand, Figure 15 shows the seasonal variations in the ozone and water-vapor concentrations of the ozone layer inside the Ozone Hole in the Antarctic region. The comparison between the variations in the water-vapor concentration on the bottom panel and the ozone concentration on the top panel also indicates the evident anti-correlation.

Thus, both outside and inside the Ozone Hole, the clear anti-correlation is found between the seasonal variations of the ozone and water distribution in the Antarctic region.

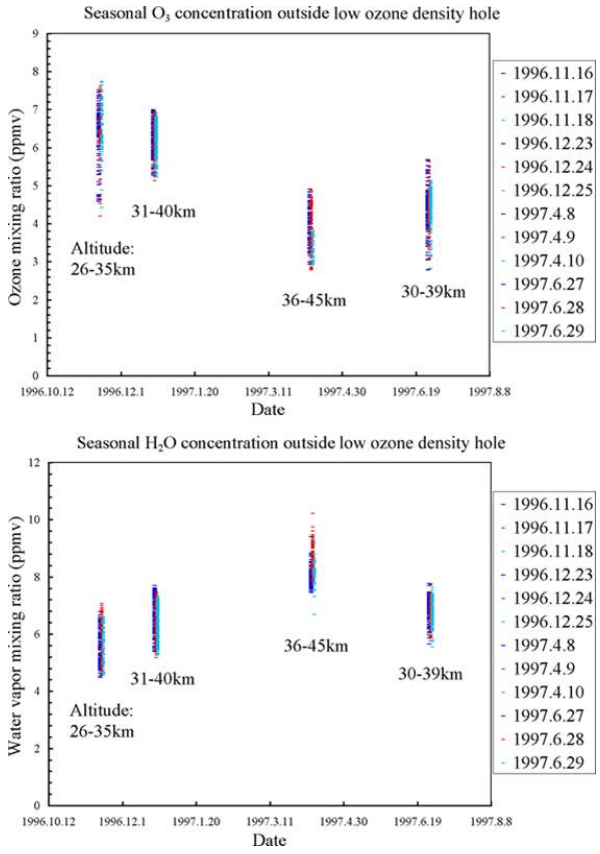

Figure 14. Seasonal variations in ozone and water-vapor concentrations of the ozone layer outside the Ozone Hole in the Antarctic region

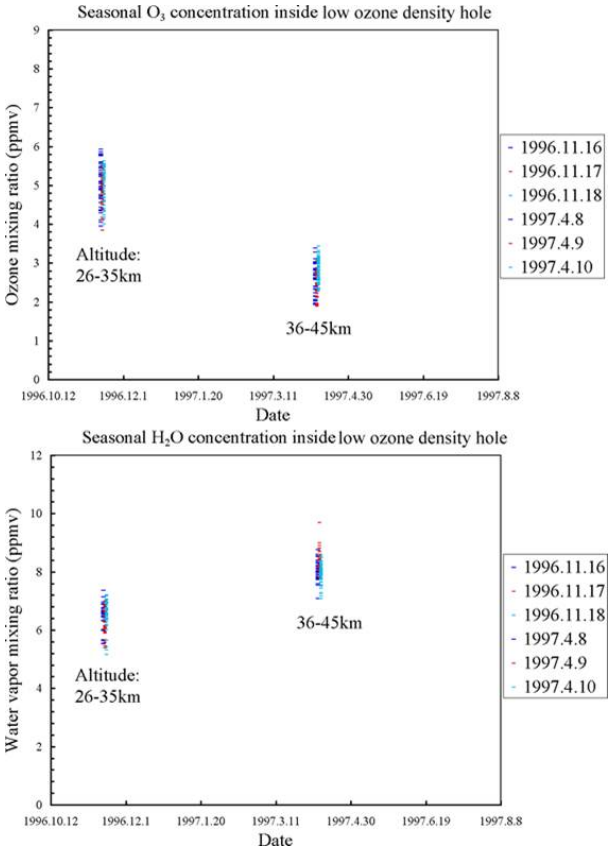

Figure 15. Seasonal variations in ozone and water-vapor concentrations of the ozone layer inside the Ozone Hole in the Antarctic region

Figure 16 shows the seasonal variations in ozone and water-vapor concentrations of the ozone layer outside the Ozone Hole in the Arctic region. Outside the Ozone Hole

in the Arctic region, the evident anti-correlation is found by the comparison between the variations in the water-vapor concentration on the bottom panel and the ozone concentration on the top panel in the figure.

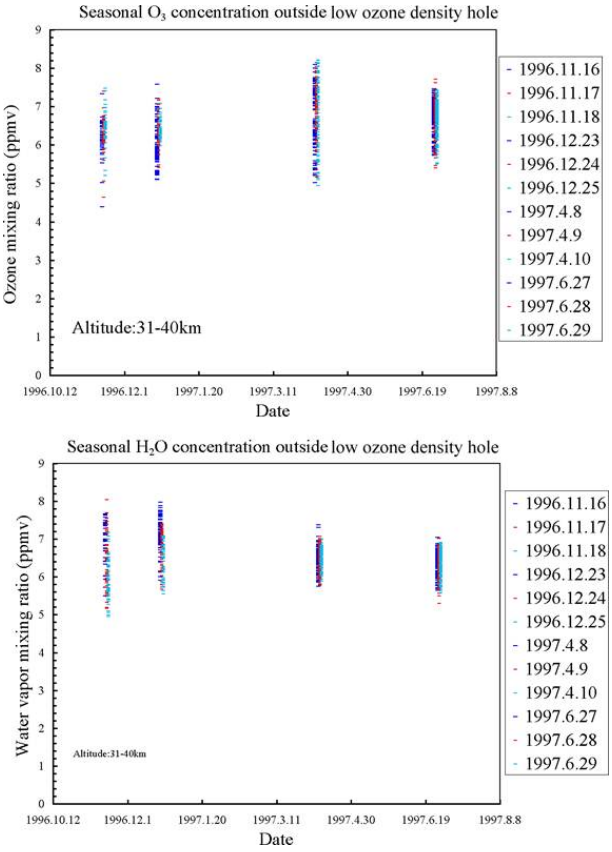

Figure 16. Seasonal variations in ozone and water-vapor concentrations of the ozone layer outside the Ozone Hole in the Arctic region

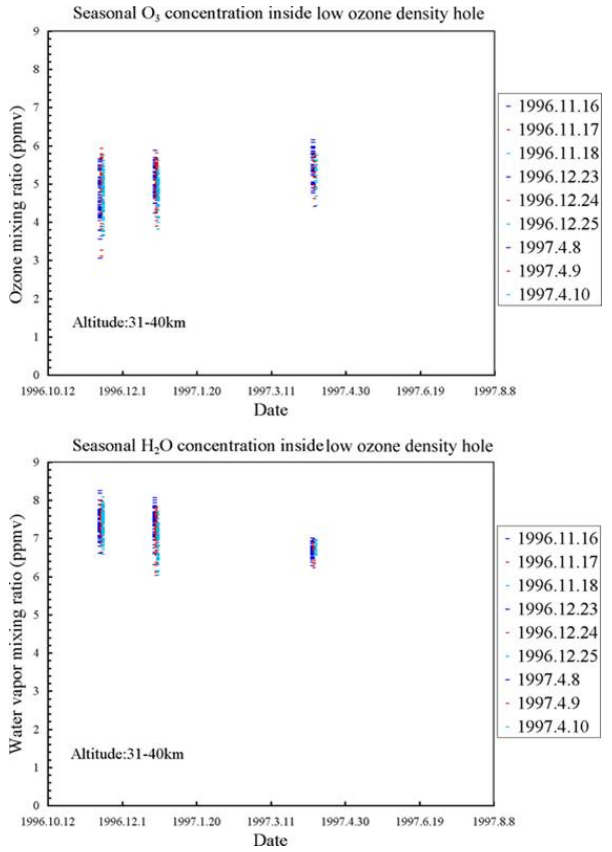

Figure 17. Seasonal variations in ozone and water-vapor concentrations of the ozone layer inside the Ozone Hole in the Arctic region

On the other hand, Figure 17 shows the seasonal variations in ozone and water-vapor concentrations of the ozone layer inside the Ozone Hole in the Arctic region. The comparison between the variations in the water-vapor concentration on the bottom panel and the ozone concentration on the top panel also indicates the evident anti-correlation.

Thus, both outside and inside the Ozone Hole, the clear anti-correlation is found between the seasonal variations of the ozone and water distribution also in the Arctic region, as well as in the Antarctic region.

As well as in the altitude-longitude maps of water vapor and ozone in the Antarctic region, in the seasonal variations in ozone and water-vapor concentrations of the ozone layers, we have confirmed the anti-correlation between the water vapor and ozone distribution both inside and outside the Ozone Hole both in the Antarctic and Arctic regions, suggesting the significance of the action of water vapor on the stratospheric ozone chemistry also in the Polar Regions.

3.2.3. Altitude Profiles of Ozone and Water Vapor Populations

As mentioned above, the interaction between ozone and water vapor is strongly suggested to be significant also in the Polar Regions. In particular, it is very interesting that the anti-correlation is observed both inside and outside the Ozone Hole. Hence, it is of great interest to investigate the different and/or common processes in the ozone chemistry between inside and outside the Ozone Hole. Since the ILAS data has the advantages in the altitude profiles of the atmospheric species, here we study the interaction between ozone and water vapor with focus on the altitude profiles of these species.

Figure 18 shows the differences in the altitude profiles of ozone and water vapor concentrations and the temperatures between inside and outside the Ozone Hole in the Antarctic region on 1 November in 1996, which are made by the ILAS data analysis. We show the light-brown iso-latitude circles including the observation points, i.e. tangential points, in the present analysis on the TOMS (Total Ozone Mapping Spectrometer) total ozone map in Figure 19. As shown in Figure 19, these observation points are placed at 74.4-74.8˚S of latitude at 44.8˚ and -163.7˚ of longitude inside and outside the Ozone Hall, respectively.

For the plots in Figure 18, we define the differences in the ozone concentrations, the water vapor concentrations, and the temperatures in the following equations:

$$\begin{aligned}&[\text{The ozone concentration difference}]\\&=[\text{An ozone concentration inside the Ozone Hole}]\\&-[\text{An ozone concentration outside the Ozone Hole}]\end{aligned} \quad (7)$$

$$\begin{aligned}&[\text{The } H_2O \text{ concentration difference}]\\&=[\text{A } H_2O \text{ concentration inside the Ozone Hole}]\\&-[\text{A } H_2O \text{ concentration outside the Ozone Hole}]\end{aligned} \quad (8)$$

$$\begin{aligned}&[\text{The temperature difference}]\\&=[\text{A temperature inside the Ozone Hole}]\\&-[\text{A temperature outside the Ozone Hole}]\end{aligned} \quad (9)$$

Hence, the plots in Figure 18 indicate the differences in the O_3 concentrations and the H_2O concentrations, and the temperatures of the region inside the Ozone Hole from those of the region outside the Ozone Hole, respectively, i.e., we will compare the ozone chemistry inside and outside the Ozone Hall through the difference in these physical factors at various altitudes.

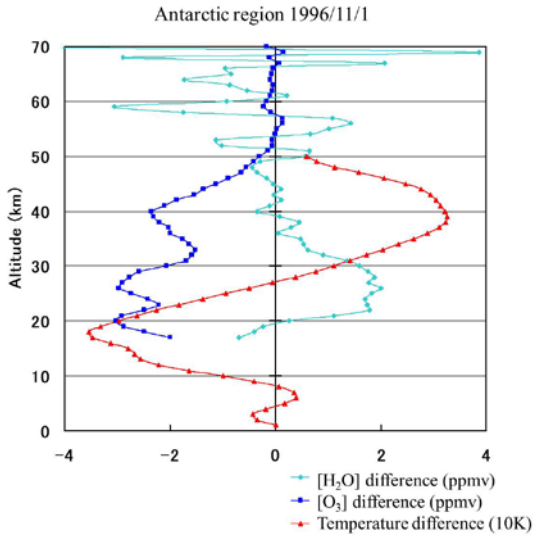

Figure 18. The ILAS data showing the differences in the altitude profiles of the water vapor and ozone concentrations and the temperatures between inside and outside the Ozone Hole in the Antarctic region on 1 November in 1996, where the abscissa indicates the differences in the H_2O and O_3 concentrations in ppmv and the temperatures in a unit of 10 K. The observation points for the present ILAS data analysis are shown in Figure 19

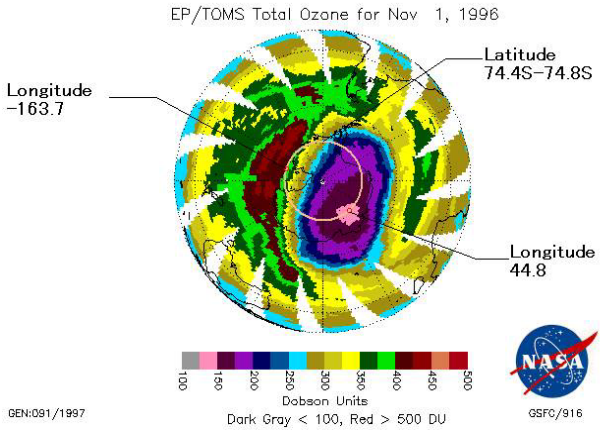

Figure 19. The observation points for the ILAS data in Figure 18, shown on the TOMS total ozone map in the Antarctic region on 1 November in 1996. The map is from NASA's TOMS [24,25], which was borne on ADEOS with ILAS. The pink-colored small concentric circle indicates the ILAS observation region, on which the tangent points are placed

As shown in Figure 19, the observation points in the present ILAS data analysis in the Antarctic region are at latitude of 74.4-74.8˚S at longitudes of 44.8˚ and -163.7˚, indicating that they are in the central region of the Ozone Hole and in the region outside the Ozone Hole, respectively; the ozone concentrations of the regions at -163.7˚ and 44.8˚ of longitudes are almost highest and lowest on the map, respectively. Hence, we can compare the ozone chemistry inside and outside the Ozone Hole at the same latitude in the same day, i.e. on 1 November in 1996.

The similar plots are made in the Arctic region. Figure 20 shows the differences in the altitude profiles of the ozone and water vapor concentrations and the temperatures between the inside and the outside of the Ozone Hole in the Arctic region on 9 April in 1997, which are made by the ILAS data analysis. For the plots in Figure 20, the observation points are shown on the NASA's TOMS total ozone map in Figure 21.

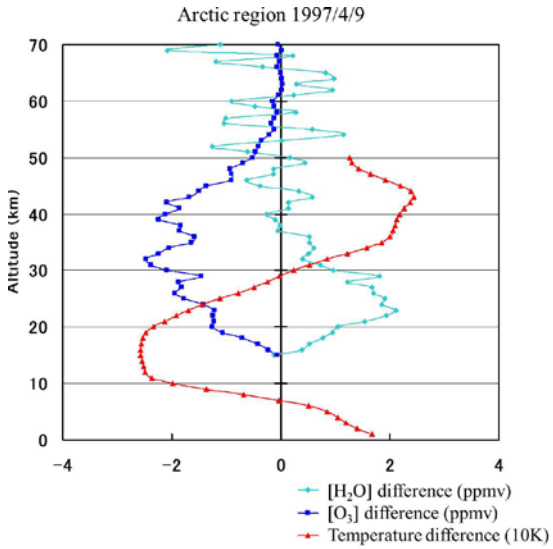

Figure 20. The ILAS data showing the differences in the altitude profiles of the water vapor and ozone concentrations and the temperatures between inside and the outside the Ozone Hole in the Arctic region on 9 April in 1997, where the abscissa indicates the differences in the H_2O and O_3 concentrations in ppmv and the temperatures in a unit of 10 K. The observation points for the present ILAS data analysis are shown in Figure 21.

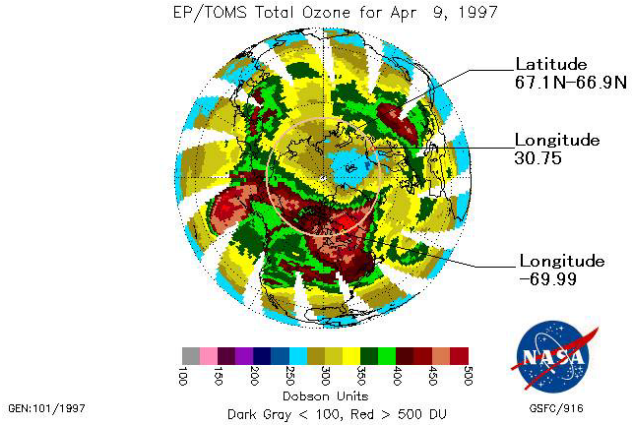

Figure 21. The observation points for the ILAS data in Figure 20, shown on the TOMS total ozone map in the Arctic region on 9 April in 1997. The map is from NASA's TOMS, which was borne on ADEOS together with ILAS [24,25]. The pink-colored small concentric circle indicates the ILAS observation region, on which the tangent points are placed

As shown in Figure 21, an Ozone Hole was evidently formed also in the Arctic region, while it is rather small and weak. Figure 21 indicates that the observation points in the present analysis in the Arctic region are at latitude of 67.1-66.9˚N at longitudes of 30.75˚ and -69.99˚, showing that they are inside and outside the Ozone Hole, respectively. The ozone concentrations at -66.99˚ and 30.75˚ of longitudes are highest and almost lowest on the map, respectively.

As shown in Figure 18 and Figure 20, in common with the Antarctic and Arctic regions, the ozone concentrations are reduced in the Ozone Hole at altitudes of 15-60 km, while the water vapor concentrations are higher at altitudes of 15-40 km in the Ozone Hole and equal at 40-50 km inside and outside the Ozone Hole. As a result, the anti-correlation is suggested between the ozone and water-vapor profiles. On the other hand, as shown in these figures, essentially in common with the Antarctic and Arctic regions, the temperatures inside the Ozone Hall are lower at altitudes of 8-28 km in the Antarctic region and at 7-29 km in the Arctic region and are higher at altitudes of 28-50 km in the Antarctic region and at 29-50 km in the Arctic region.

3.2.4. Correlations between Ozone and Water Vapor Concentrations

In the previous sections, i.e. in Sections 3.2.1-3.2.3, the significant interaction between ozone and water vapor is suggested. In this section, to investigate it more in detail, we will starts from studying the correlations between the ozone and water vapor concentrations by the plots of the ozone concentration as a function of the water vapor concentration.

As shown in Figure 22 and Figure 23, the ozone concentration is plotted as a function of the water vapor concentration at the altitudes of 25 km and 20 km, respectively, in the Antarctic region.

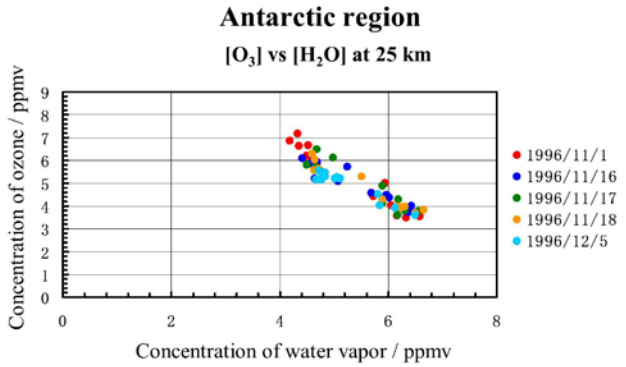

Figure 22. The plot of ozone concentration as a function of water vapor concentration at 25 km of altitude in the Antarctic region on 1 November – 5 December in 1996 by using ILAS data

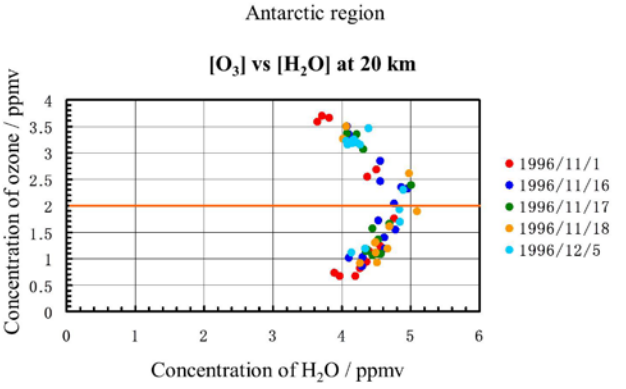

Figure 23. The plot of ozone concentration as a function of water vapor concentration at 20 km of altitude in the Antarctic region on 1 November – 5 December in 1996 by using ILAS data

As shown in Figure 22, it is found that the ozone concentration shows the clear anti-correlation with the water vapor concentration at 25 km. On the other hand, as shown in Figure 23, the correlation between the ozone and water vapor concentrations at 20 km is found to be quite interesting; the ozone concentration is proportional to the water vapor concentration for the ozone concentration less than 2 ppmv, while the ozone concentration is inversely proportional to the water vapor concentration for the ozone concentration higher than 2 ppmv. Since we have confirmed that the region with the ozone concentration higher than 2 ppmv is placed outside the Ozone Hole and the region with the ozone concentration lower than 2 ppmv is placed inside the Ozone Hole, it is found that the ozone concentration is proportional to the water vapor concentration inside the Ozone Hall, while they show the anti-correlation outside it.

Figure 24 shows the plot of the ozone concentration as a function of the water vapor concentration at 30 km in the Antarctic region, indicating that the ozone concentration is inversely proportional to the water vapor concentration for the ozone concentration higher than 5 ppmv and constant with an increase in water vapor concentration for the ozone concentration around 5 ppmv. We also made the similar plots at 35, 40, 45, and 50 km. As a result, the inversely proportional relation, which is rather similar to the one at 30 km, is obtained at 35 km, while the correlation is not clear at 40 km and is in linear proportion at 45 and 50 km.

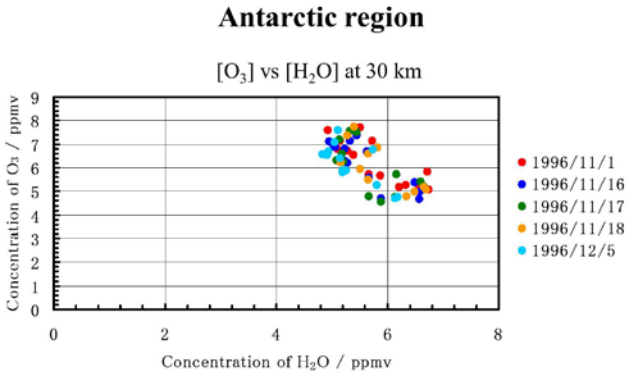

Figure 24. The plot of ozone concentration as a function of water vapor concentration at 30 km of altitude in the Antarctic region on 1 November – 5 December in 1996 by using ILAS data

Furthermore, the HNO_3 concentration is plotted as a function of the H_2O concentration at 20 km, as shown in Figure 25. The HNO_3 concentration is proportional to the H_2O concentration for the HNO_3 concentration lower than 5 pptv, while no systematic correlation is observed for the HNO_3 concentration higher than 5 pptv.

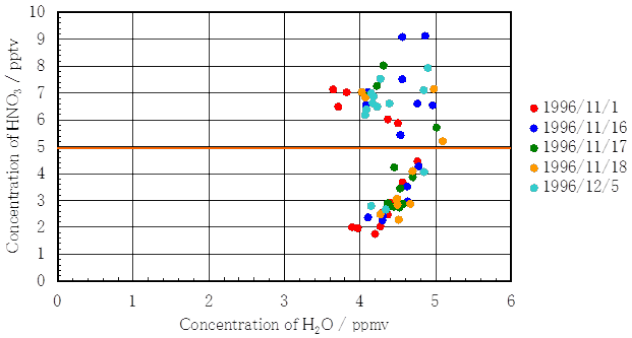

Figure 25. The plot of nitric acid concentration as a function of water vapor concentration at 20 km of altitude in the Antarctic region on 1 November – 5 December in 1996 by using ILAS data

Furthermore, the HNO_3 concentration is plotted as a function of the ozone concentration at 20 km, as shown in Figure 26. The HNO_3 concentration is clearly proportional to the O_3 concentration for the HNO_3 concentration lower than 5 pptv, while the correlation disappears for the HNO_3 concentration higher than 5 pptv, indicating that the HNO_3 concentration does not change with an increase in the ozone concentration.

As seen in Figure 26, the HNO_3 concentration of 5 pptv corresponds to the ozone concentration of 2 ppmv. Hence, as discussed with Figure 23, since the region with the ozone concentration lower than 2 ppmv is in the Ozone Hole and the one with the O_3 concentration higher than 2 ppmv is outside the Ozone Hole, as for the HNO_3 data in Figure 25 and Figure 26, the clear linear correlation of the HNO_3 concentration with the H_2O and O_3 concentrations is found only inside the Ozone Hole and no clear correlation is observed among them outside it.

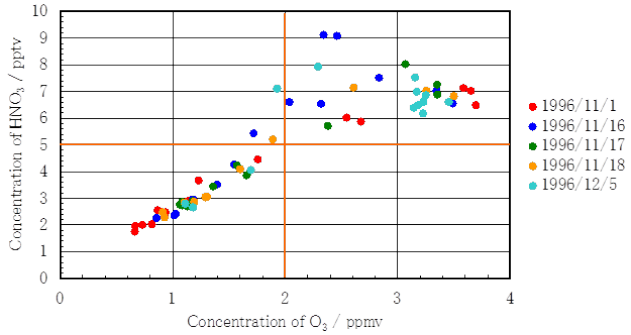

Figure 26. The plot of the nitric acid concentration as a function of the ozone concentration at 20 km of altitude in the Antarctic region on 1 November – 5 December in 1996 by using ILAS data

Besides the analysis in the Antarctic region, the similar analysis was made in the Arctic region. For instance, as shown in Figure 27, we have studied the correlation between the ozone and water vapor concentrations. The result is compared with the one in Figure 23, indicating that both the results in Figure 27 and Figure 23 show the anti-correlation for the ozone concentration higher than 2 ppmv, while the result in Figure 23 shows the proportional relation for the ozone concentration less than 2 ppmv, where the data is unavailable in Figure 27.

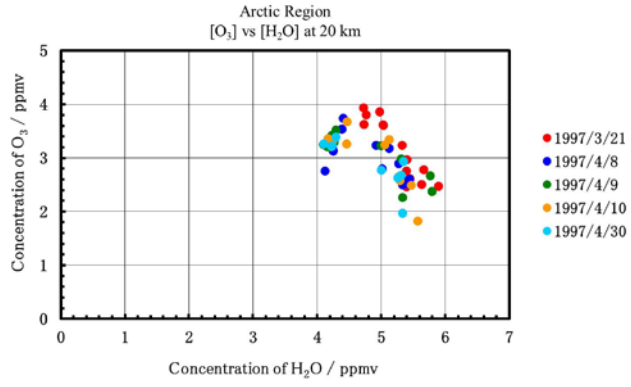

Figure 27. The plot of the ozone concentration as a function of the water vapor concentration at 20 km of altitude in the Arctic region on 21 March – 30 April in 1997 by using ILAS data

Furthermore, the analysis in the Arctic region indicates the weak anti-correlation between the ozone and water vapor concentrations at altitudes of 25, 30, and 35 km. Yet no clear systematic correlation is observed at 40 km. The correlation is in linear proportion at 45 and 50 km. Thus it is found that the correlations between the ozone and water vapor concentrations at the individual altitudes are essentially same between in the Arctic and Antarctic regions.

3.2.5. Discussion on the Correlations between Ozone and Water Vapor Concentrations

Based on the results in Sections 3.2.1-3.2.4, let us discuss the interaction between ozone and water vapor in the Polar Regions in this section.

As shown in Figure 13 and Figure 14-Figure 17, since the anti-correlation between the ozone and water vapor concentrations is found to be formed longitudinally, i.e. spatially, and seasonally, i.e. temporally, in the Polar Regions, the HO_x species can be regarded as the essential chemicals in the ozone chemistry in the Polar Regions. The present results, as well as the ones in the equatorial regions as discussed in Section 3.1, agree well with the surprising facts that the HO_x cycle is the dominant mechanism rather than the NO_x cycle, which were found by the Stratospheric Photochemistry Aerosols and Dynamics Expedition (SPADE) in 1993 and the Airborne Southern Hemisphere Ozone Experiment (ASHOE) in 1994.

On the other hand, in the Polar Regions, we have to take account of the characteristic local ozone distribution, i.e., the Ozone Holes, which are closely related to the Polar Vortexes. As shown in Figure 18 and Figure 20, the differences in the ozone and water vapor concentrations and the temperatures inside and outside the Ozone Hole indicate that the ozone concentration is lower and the water vapor concentration is higher inside the Ozone Hole at altitudes of ca20-35 km commonly in the both Polar Regions, i.e., the anti-correlation between the ozone and water vapor concentrations is observed. On the other hand, at the altitudes of 40-50 km, while the ozone concentration inside the Ozone Hole is lower than the one outside it, the water vapor concentrations inside and outside the Ozone Hole are almost equal. Furthermore, the temperatures inside the Ozone Hole are lower than the ones outside it at the altitudes lower than ca25 km, while they are higher at the altitudes higher than it. Thus, the discussion on these results will give us the significant aspects of the ozone chemistry in the Polar Regions.

At the beginning, let us discuss more in detail the results in the Antarctic Region in Figure 18. In the case, the temperatures at the altitudes of 9-28 km are lower inside the Polar Vortex, where the ozone concentration greatly decreases at the same altitudes. Because of the low temperature inside the Polar Vortex, we suppose that the H_2O tends to be present as liquids and/or solids including usually HNO_3 rather than as vapors at the altitudes in winter. The H_2O condensation like this will enhance the heterogeneous chemical reactions on the liquid and solid H_2O including HNO_3, which are known to decrease the ozone concentration more efficiently. In spring, the water vapor concentration will increase through the partial evaporation from the liquid and solid H_2O including HNO_3, and yet the heterogeneous chemical reactions on the liquid and solid H_2O containing HNO_3 will be still active. As a result, in spring, at the altitudes of 20-28 km inside the Polar Vortex, the temperature is lower, the

ozone concentration is lower, and the water vapor concentration is higher, as compared with those outside the vortex, as shown in Figure 18.

On the other hand, at the altitudes of 28-50 km, the temperature inside the Ozone Hole is higher than the one outside it, as shown in Figure 18. Hence, the H_2O condensation is supposed to be not the predominant process at the altitudes inside the Polar Vortex even in winter. Therefore the water vapor concentrations inside and outside the Ozone Hole are almost equal, as confirmed in Figure 18. Nevertheless, the ozone concentration is lower inside the Ozone Hole than outside it. We suppose that the mechanism for it is due to the chemical processes; since the temperature is higher inside the Ozone Hole, the ozone depletion reactions in the gas phase will be enhanced there. Besides the enhancement of the chemical processes, the effect of fluid dynamics might be significant.

Similarly, let us discuss the results in the Arctic Region in Figure 20. As shown in Figure 20, inside the Polar Vortex, the temperature is lower at the altitudes of 7-29 km, the water vapor concentration is higher at altitudes of 15-37 km, and the ozone concentration is lower at the altitudes of 15-60 km. In spring, the water vapor concentration increases by the evaporation from the H_2O in the condensed phases; this is formed in winter. As a result, at the altitudes of 15-30 km inside the Ozone Hole, the ozone concentration decreases through the gas-phase chemical reactions between ozone and water vapor on the surface of the condensed H_2O. On the other hand, at the altitudes of 30-60 km, the gas-phase ozone depletion reactions with HO_x species are enhanced inside the Ozone Hole, since the temperature is higher there, in spite of the fact that the water vapor concentrations inside and outside the Ozone Hole are equal.

Now let us move to the discussion on the results in Figure 22-Figure 27.

As shown in Figure 22 and Figure 24, in the Antarctic Region, the ozone concentration decreases with an increase in the water-vapor concentration at the altitudes of 25 and 30 km. To discussing this anti-correlation between the ozone and water-vapor concentrations, we will be able to apply Scheme 1 in Section 3.1, which consists of Processes (2)-(6) and is a gas-phase HO_x catalytic reactions scheme.

On the other hand, as shown in Figure 23, the correlation between the ozone and water vapor concentrations is characteristic at 20 km; it is the anti-correlation and the proportional correlation for the ozone concentrations higher and lower than 2 ppmv, respectively. Since it is found that the regions with the ozone concentration higher and lower than 2 ppmv are outside and inside the Ozone Hole, respectively, the ozone chemistry outside the Ozone Hole is expressed in terms of the gas-phase HO_x catalytic reactions of Scheme 1, as well as the results at the altitudes of 25 and 30 km in Figure 22 and Figure 24.

On the other hand, we will apply following Scheme 2 to the chemistry inside the Ozone Hole at 20 km in Figure 23.

Scheme 2:

In winter,

$$\begin{aligned} &\mathrm{ClONO_2\,(gas) + H_2O\ (solid) \rightarrow} \\ &\mathrm{HOCl\ (gas) + HNO_3\,(solid)} \end{aligned} \quad (10)$$

In spring,

$$\mathrm{HOCl} + h\nu \rightarrow \mathrm{OH} + \mathrm{Cl} \quad (11)$$

$$\mathrm{Cl} + \mathrm{O_3} \rightarrow \mathrm{ClO} + \mathrm{O_2} \quad (12)$$

$$\mathrm{(ClO)_2} + h\nu \rightarrow \mathrm{Cl} + \mathrm{ClOO} \quad (13)$$

$$\mathrm{ClOO} + \mathrm{M} \rightarrow \mathrm{Cl} + \mathrm{O_2} + \mathrm{M} \quad (14)$$

In winter, PSCs (Polar Stratospheric Clouds) are formed around the altitudes of 20 km inside the Polar Vortex. PSCs consist of supercooled ternary solution (STS), nitric acid dihydrate (NAD), nitric acid trihydrate (NAT), and/or nitric acid pentahydrate (NAP), depending on the atmospheric temperature. On the surface of the PSCs, the inhomogeneous reaction of Process (10) occurs. Then, in spring, the solar radiation causes the emission of Cl by the photolysis of HOCl in Process (11). It is followed by Processes (12)-(14); through these processes, the ozone concentration is reduced. After all, both the H_2O and ozone concentrations decrease through Processes (10) and (12), respectively. Thus, in Scheme 2, the ozone and water vapor concentrations are in the proportional correlation.

Furthermore, since dehydration in Process (10) yields HNO_3, the HNO_3 and H_2O concentrations will be in the proportional correlation. In fact, in Figure 25, we can confirm the proportional correlation between them in the region where the HNO_3 concentration is less than 5 pptv. As shown in Figure 26, the region with the HNO_3 concentration less than 5 pptv coincides with the region with the ozone concentration less than 2ppmv, i.e., the region inside the Ozone Hole. Thus, it will be appropriate to consider that the ozone chemistry inside the Ozone Hole at 20 km is due to Scheme 2.

The ozone chemistry in the Arctic Region will be similarly discussed as well as in the Antarctic Region. Yet, the Polar Vortex in the Arctic Region, and hence the Ozone Hole, as seen in Figure 21, are rather weak. The correlation between the ozone and water vapor concentrations in Figure 16 and Figure 17 looks rather weak. In fact, as shown in Figure 27, in the correlation between the ozone and water vapor concentrations at 20 km in the Arctic region, the proportional correlation at the ozone concentration less than 2 ppmv in the Antarctic Region in Figure 23 cannot be observed, indicating that the ozone depletion in the Ozone Hole in the Arctic Region is to a lesser degree, as compared with the one in the Antarctic Region.

3.3. Total Column Ozone Maps by ILAS

TOMS [24,25] has provided the beautiful Ozone-Hole maps in the Polar Regions, measuring the back-scattered ultra-violet solar radiation from the atmosphere. Because of the back-scattered solar radiation measurements in TOMS, there are unobservable regions in the whole-day-night sides in the Polar Regions in winter. On the other hand, ILAS measures the infrared spectra of ozone by a solar occultation method, providing fourteen vertical profiles of ozone density at definite latitudes in the Arctic and Antarctic Regions for a day. Since these latitudes are on the day-night boundaries, even when they are in the whole-day-night sides for TOMS in winter, the ILAS data seems to be possible to add the information partially to the TOMS maps in its unobservable regions of the whole-day-

night-sides. Hence, in the present paper, here we study making the total ozone maps by using the ILAS data.

Figure 28 shows the calendar comparing the TOMS and ILAS observation schedules. On the bottom panel in the figure, the ILAS observation period, which is since 30 October 1996 to 29 June 1997, is shown by a black-colored solid line with black-colored letters. On the top panel in the figure, the TOMS data availability during the ILAS observation period is shown by the red, green, blue-colored lines and letters. The red-colored line and letters indicate the TOMS-data available period in the Antarctic Region, which is since 30 October 1996 to 12 March 1997. After the period, the TOMS data is unavailable, as shown by the green dashed line and letters. In the Arctic Region, while the TOMS data is unavailable until 28 February 1997, as shown by the green dashed line, it is available since 29 February 1997 to 29 June 1997, as shown by the blue solid line and letters. Therefore, we will make the total ozone maps for these TOMS-data unavailable periods.

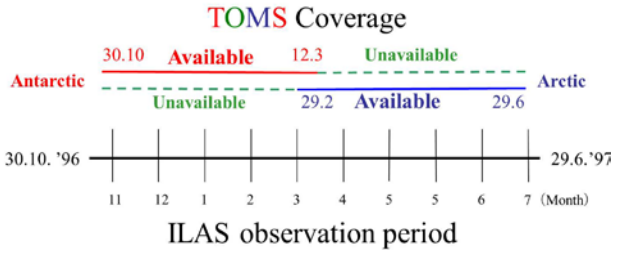

Figure 28. TOMS-data available (red and blue solid-lines) and unavailable (green dashed lines) periods and ILAS observation period (a black line)

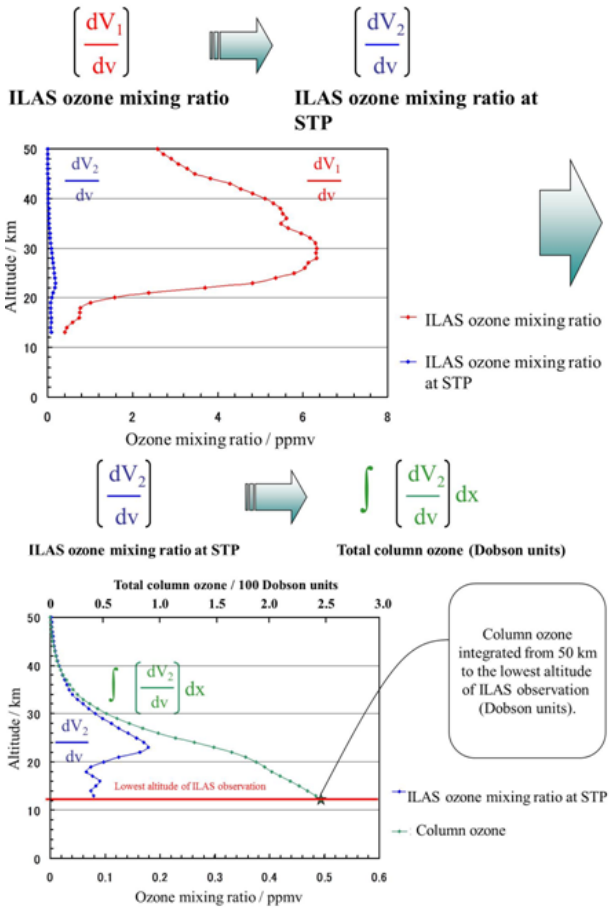

Figure 29. Process of making the total ozone map from the ILAS data

The process for making the total ozone map from the ILAS data is schematically shown in Figure 29. As shown on the top panel in the figure, the ozone mixing ratio of the ILAS data is transformed to the ozone mixing ratio at STP (standard temperature and pressure) by using the UKMO (UK Met Office) data [26]. Typically, the transformation is made at altitudes of 14-50 km, since the ILAS and UKMO data are available at altitudes of ca14-70 km and 1-50 km, respectively. In the transformation, V_1 and V_2 are the volumes at the ILAS tangential point with a temperature of T_1 and a pressure of P_1 and at STP with a temperature of T_2 = 0 K and a pressure of P_2 = 1 atm, respectively. The equation of Boyle-Charles rule, $(P_1V_1/T_1) = (P_2V_2/T_2)$, is differentiated by a variable of volume v and then the ozone mixing ratio (dV_1/dv) by the ILAS data is transformed to the one (dV_2/dv) at STP.

As shown on the bottom panel in Figure 29, the integration of the ILAS ozone mixing ratio at STP over the altitudes from typically 14 to 50 km gives the total column ozone in Dobson unit, where the lowest limit of the altitude depends on the ILAS data. We shall call this $[ILAS]_{column}$ and the TOMS data $[TOMS]_{column}$.

In Figure 30-Figure 33, $[ILAS]_{column}$ and $[TOMS]_{column}$ are compared. In these figures, $[ILAS]_{column}$ and $[TOMS]_{column}$ are indicated by the green and red solid lines, respectively. In these figures, for instance, "ILAS: 15-50 km" in the squares indicates that the integration is made at the altitudes from 15 km to 50 km. Furthermore, for instance, "TOMS/ILAS: 1.235" in the squares indicates that the ratio of the TOMS data to ILAS total column ozone is 1.235. It is found that the ratio is always higher than one, since $[ILAS]_{column}$ is always lower than $[TOMS]_{column}$.

The fact that $[ILAS]_{column}$ is always less than $[TOMS]_{column}$ is due to that the altitude range for the integration is limited in the present analysis, i.e., for the exact analysis, the integration has to be made from 0 to infinity of the altitude. Thus, since the column ozone at the altitudes less and higher than the altitudes of the minimum and maximum limits of the integration, respectively, is omitted, $[ILAS]_{column}$ is always less than $[TOMS]_{column}$. On the other hand, the fact that the curves of $[ILAS]_{column}$ and $[TOMS]_{column}$ are rather similar suggests that the scaled $[ILAS]_{column}$ by multiplying $[ILAS]_{column}$ and a scaling factor will be a good improved ILAS total column ozone. By using the scaling factors, which equal the ratios $[TOMS]_{column}/[ILAS]_{column}$, the scaled $[ILAS]_{column}$ are thus obtained and shown by the blue solid lines in Figure 30-Figure 33. As seen in the figures, the scaled $[ILAS]_{column}$ agrees well with $[TOMS]_{column}$. Thus, the present scaling method is found to give fairly exactly the quantity of the ILAS total column ozone.

On the other hand, since our final aim is to make the ozone maps in the regions lacking the $[TOMS]_{column}$ data, we cannot calculate the scaling factor from the ratios $[TOMS]_{column}/[ILAS]_{column}$ in the case. Hence, in advance of the analysis in the region lacking the TOMS data, we try to make the universal scaling factors by using the ILAS and TOMS data in the cases, where both the data are available.

At the beginning of estimating the universal scaling factors, $[TOMS]_{column}/[ILAS]_{column}$ is plotted as a function of the lowest altitude of the integration of the ILAS data, as shown in Figure 34. In the figure, the averaged curves in these plots are obtained with the standard deviations

both in the Antarctic and Arctic Regions. From the averaged curves, we read the universal scaling factors at the individual lowest altitudes of the ILAS data. As the precision of the universal scaling factors, the standard deviations will be appropriate to estimating the quantitative values of the total column ozone by using the universal scaling factors.

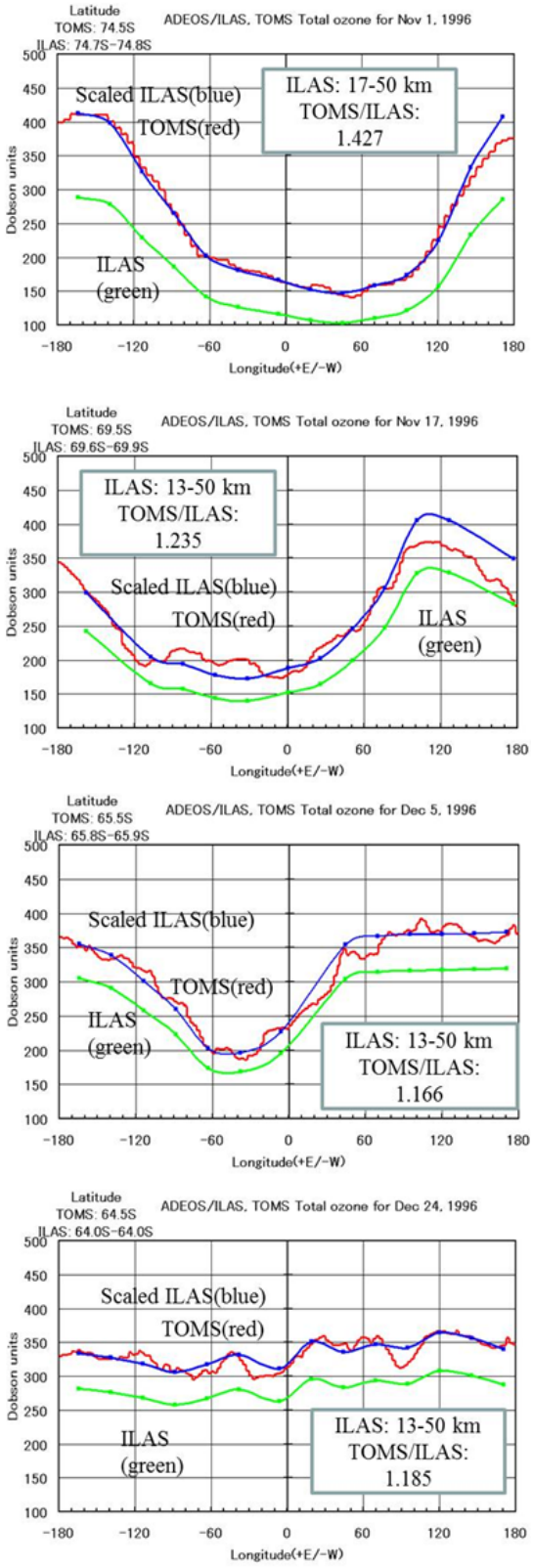

Figure 30. $[ILAS]_{column}$ (green lines), the scaled $[ILAS]_{column}$ (blue lines), and $[TOMS]_{column}$ (red lines) in the Antarctic Region: from the top to bottom panels, on 1 and 17 November and 5 and 24 December 1996, respectively

Thus, we can obtain the good method to estimate quantitatively the total column ozone from the ILAS data in the regions, where the TOMS data is unavailable. The results of the analysis are shown in Figure 35-Figure 38. Before discussing them, let us discuss a little more with Figure 34.

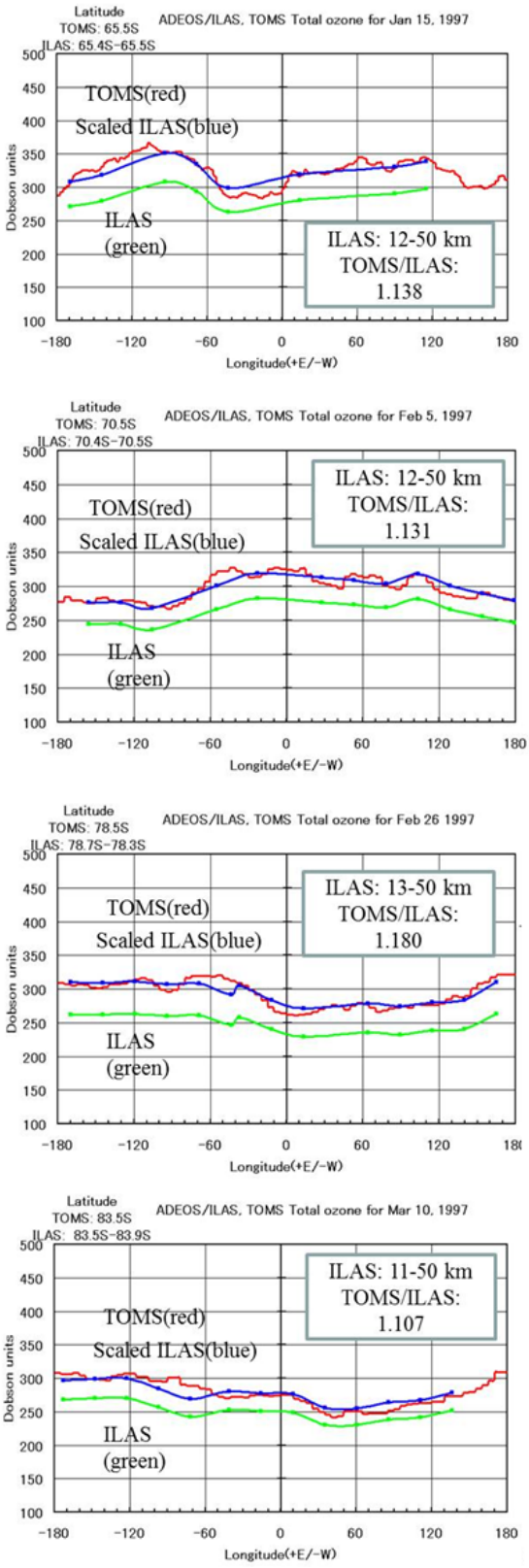

Figure 31. $[ILAS]_{column}$ (green lines), the scaled $[ILAS]_{column}$ (blue lines), and $[TOMS]_{column}$ (red lines) in the Antarctic Region: from the top to bottom panels, on 15 January, 5 and 26 February, and 10 March 1997, respectively

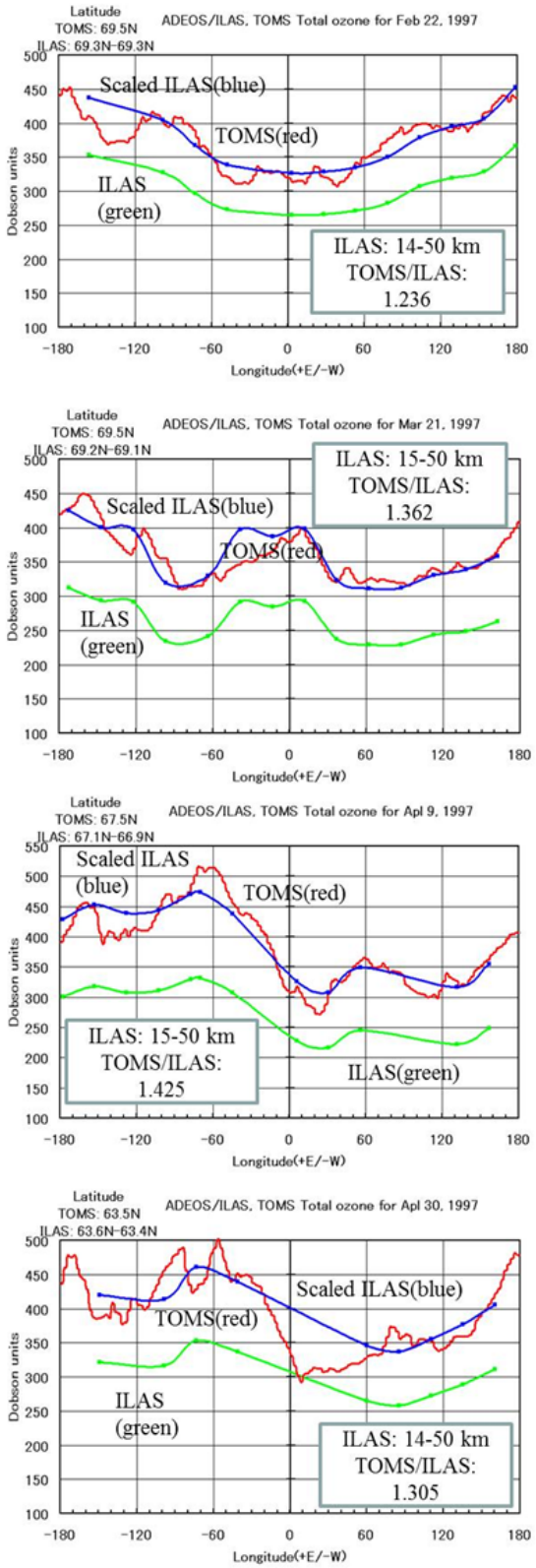

Figure 32. $[ILAS]_{column}$ (green lines), the scaled $[ILAS]_{column}$ (blue lines), and $[TOMS]_{column}$ (red lines) in the Arctic Region: from the top to bottom panels, on 22 February, 21 March, and 9 and 30 April 1997, respectively

As shown in Figure 34, the scaling factors decrease with a decrease in the lowest limit altitude of the integration of the ILAS data, approaching one with a decrease in the lowest altitude, and the standard deviations also decrease with a decrease in the lowest altitude of the ILAS data, indicating that neglecting the data under the lowest altitude of the ILAS data is the significant factor for the reduction of the total column ozone calculated with the ILAS data and that the total column ozone maps with the accurate structures will be deduced from the ILAS data by use of the universal scaling factor.

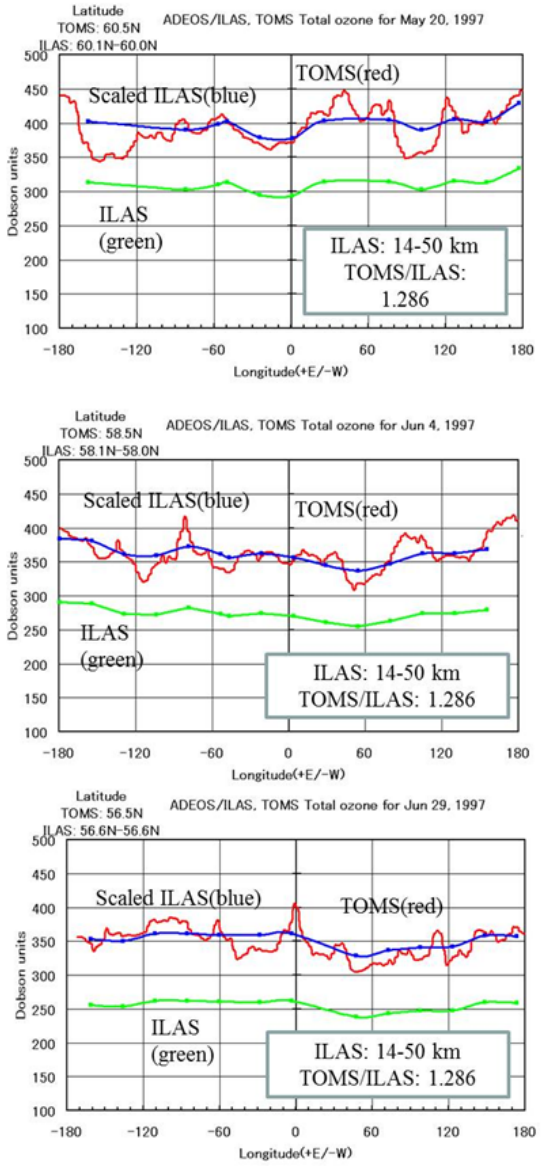

Figure 33. $[ILAS]_{column}$ (green lines), the scaled $[ILAS]_{column}$ (blue lines), and $[TOMS]_{column}$ (red lines) in the Arctic Region: from the top to bottom panels, on 20 May and 4 and 29 June 1997, respectively

Furthermore, Figure 30-Figure 33 indicate that, while the scaled ILAS lines agree well with the TOMS lines, the latter have the fine structures. The ILAS data has no adequate spatial resolution to reproduce the fine structures, since the ILAS data has only the 14 observation points for a day.

The total column ozone curves estimated from the ILAS data by using the universal scaling factors in the regions lacking the TOMS data in the Antarctic and Arctic Regions are shown in Figure 35 and Figure 36, respectively. In these figures, the thick solid blue lines indicate the total column ozone deduced from the ILAS data with the universal scaling factors, which is labeled by "Normalized ILAS" in the figures, and the thin solid blue lines on their both sides indicate the values after the addition and subtraction of the standard deviations. As shown in the figures, it is found that the standard deviation is much less than both the total column ozone, i.e. Normalized ILAS and ILAS, indicating that the present method by using the

universal scaling factors is appropriate to our purpose, satisfying it adequately.

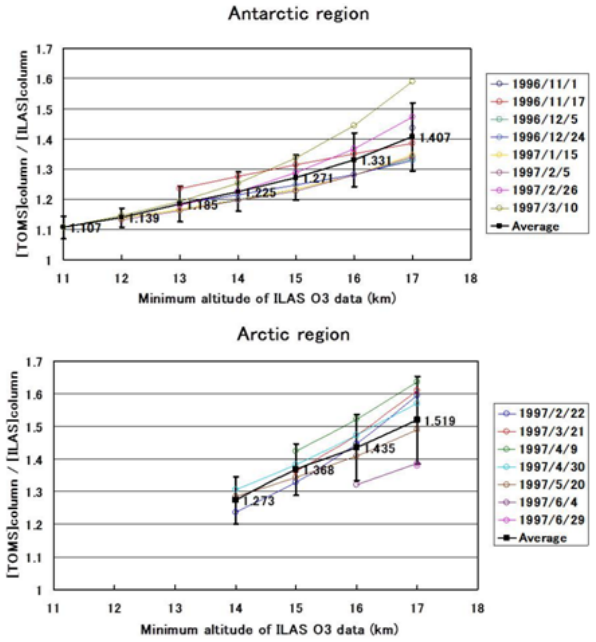

Figure 34. Plots of $[ILAS]_{column}/[TOMS]_{column}$ as a function of minimum altitude of the ILAS ozone data in the Antarctic and Arctic Regions, on the top and bottom panels, respectively, where the observation dates of the ILAS data are shown in the frames as year/month/day. The error bars indicate the standard deviations added to and subtracted from the averaged curves (the black solid lines with the closed squares)

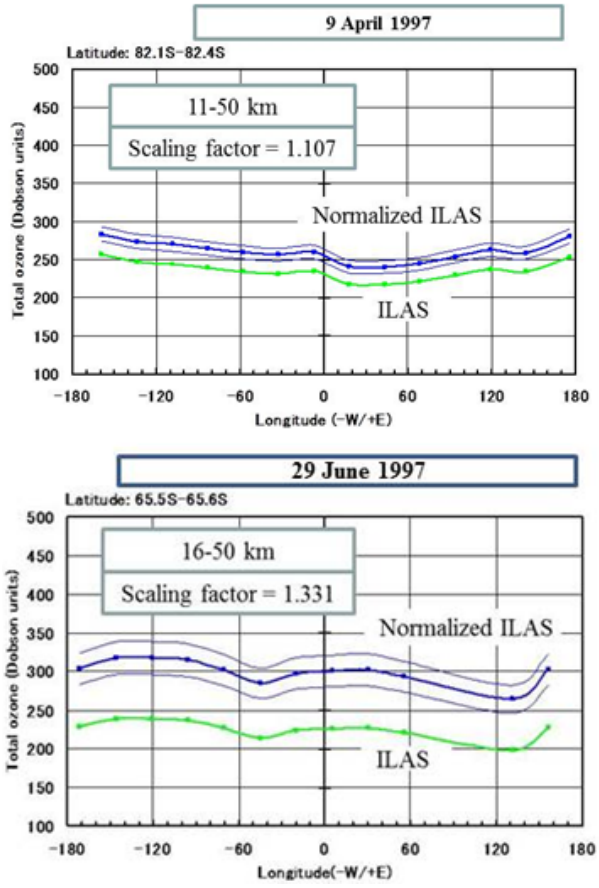

Figure 35. The total column ozone as a function of longitude for the ILAS data and the normalized ILAS data, which is obtained with the universal scaling factors, in the Antarctic Region on 9 April 1997 (top panel) and 29 June 1997 (bottom panel)

Hence, let us make the total ozone maps by superimposing the present results on the TOMS ozone maps. The results in the Antarctic and Arctic Regions are shown in Figure 37 and Figure 38, respectively. These figures indicate that the circles formed from the normalized ILAS ozone maps in Figure 35 and Figure 36 are superimposed on the blank regions of the TOMS total ozone maps. Figure 37 and Figure 38 indicate the appropriate continuity between the ozone distribution in the normalized ILAS ozone map and the TOMS total ozone map in any cases. Simultaneously, it is found that the normalized ILAS ozone maps are not only the ones simply extrapolated from the TOMS ozone maps but also the ones indicating the new structures, which will be hard to be imagined from the TOMS ozone maps, in the regions lacking the TOMS ozone maps; nevertheless, these new structures look in good accord with the TOMS ozone maps. Hence, the present study to add the ILAS ozone maps to the TOMS maps is found to be of great interest in the scientific view.

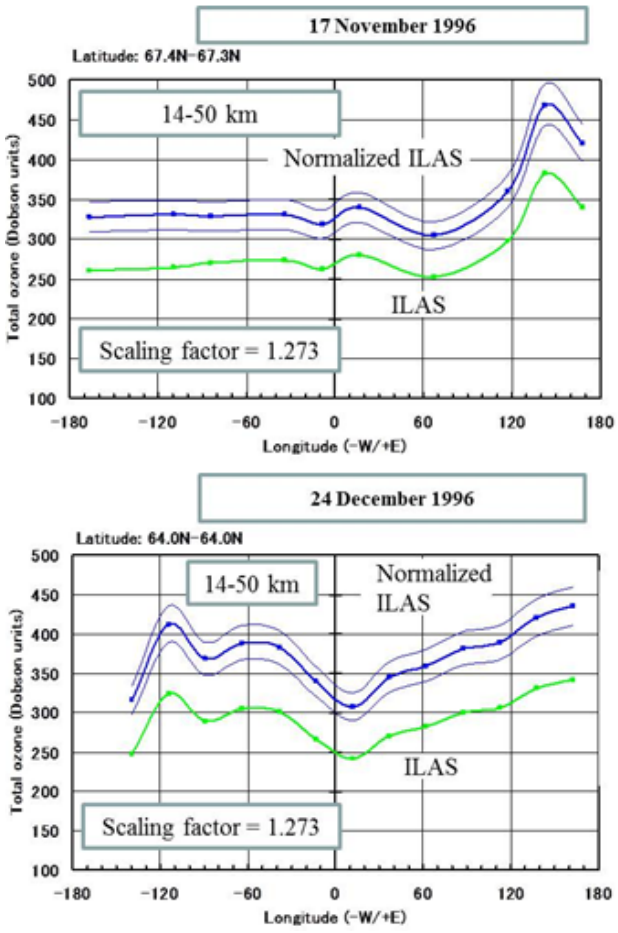

Figure 36. The total column ozone as a function of longitude for the ILAS data and the normalized ILAS data, which is obtained with the universal scaling factors, in the Arctic Region on 17 November 1996 (top panel) and 24 December 1996 (bottom panel)

In spite of the fact that the normalized ILAS ozone maps give the very significant information to the TOMS ozone maps, we consider that the use of not only the ILAS and ILAS-II data but also other satellite data will be very effective in view of extending the spatial and temporal coverage. In particular, we consider that the integration of the data from other significant sensors, e.g., like the SAGE series will be very effective for it.

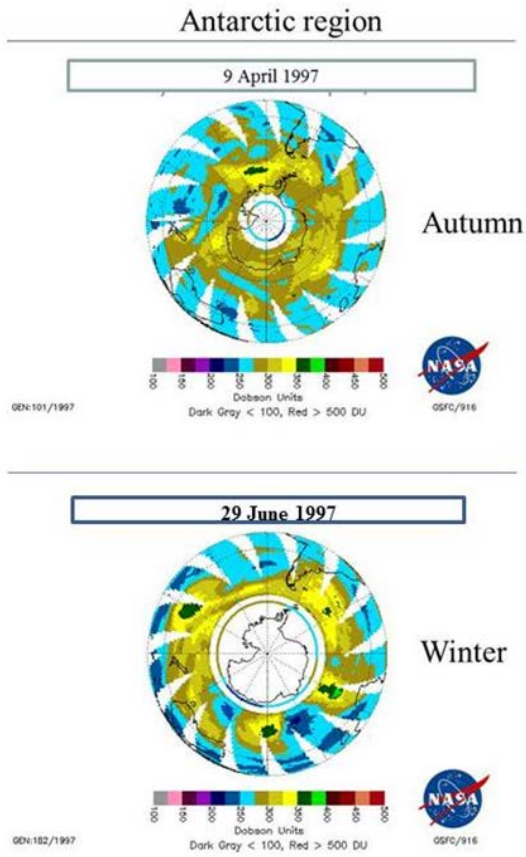

Figure 37. The circular total column ozone maps deduced from the normalized ILAS data with use of the universal scaling factors are superimposed on the TOMS ozone maps in the Antarctic Region on 9 April 1997 (top panel) and 29 June 1997 (bottom panel)

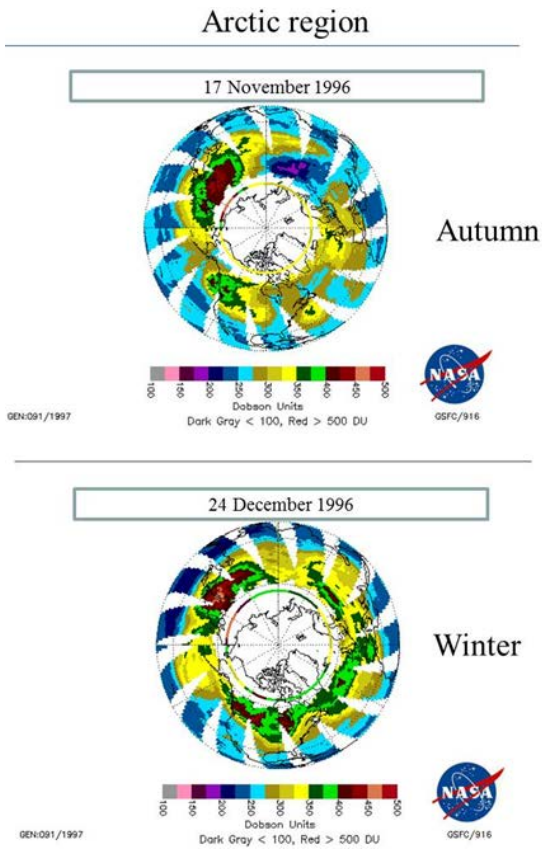

Figure 38. The circular total column ozone maps deduced from the normalized ILAS data with use of the universal scaling factors are superimposed on the TOMS ozone maps in the Arctic Region on 17 November 1996 (top panel) and 24 December 1996 (bottom panel)

4. Conclusion

Here the stratospheric ozone chemistry has been studied focusing on the action of water vapor by using the data of the satellite-borne solar occultation infrared spectrometers LAS and ILAS.

By the analysis of the LAS data, we have studied the interaction of water vapor on the stratospheric ozone chemistry in the northern low latitude region in spring. We have found the anti-correlation between the ozone and water vapor concentrations at the altitudes of 30 and 40 km, where the ultra-violet solar radiation significantly contributes to the stratospheric ozone chemistry, indicating that water vapor evidently decreases the ozone concentration with the aid of the ultra-violet solar radiation there in spring. We also have confirmed that the northern low latitude region is the significant place for water vapor to be transferred from the troposphere to the stratosphere in spring through the upstream. In fact, ITCZ is known to be placed there in spring, and hence, in the present study, it will be appropriate to consider that water vapor enters from the troposphere to the stratosphere through the upstream. Thus, the ozone chemistry in the northern low latitude regions in spring has been successfully discussed with Scheme-1 including the HO_x cycle significantly.

Furthermore, we have studied the ozone chemistry in the Polar Regions, focusing on the interaction between ozone and water vapor, by the analysis of the ILAS data. First, we have confirmed the clear anti-correlation between the water vapor and ozone distribution in their altitude-longitude maps and in their seasonal variations, i.e. in the spatial and temporal viewpoints, respectively. Then, we have compared the altitude distribution of the ozone and water vapor concentrations and of the temperatures inside and outside the Ozone Hole, which is a typical local characteristic ozone distribution in the Polar Regions. In fact, the anti-correlation has been confirmed between the difference in the ozone altitude distribution inside and outside the Ozone Hole and the one in the water-vapor altitude distribution inside and outside it. Besides, it has been found that the anti-correlation is affected by the temperature difference. Furthermore, we have studied the interrelationships between the ozone and water vapor concentrations, the water vapor and nitric acid concentrations, and also the ozone and nitric acid concentrations at various altitudes. The results have been appropriately discussed by Schemes 1 and 2. In particular, Scheme 2 is the specific mechanism in the Polar Regions, including the significant contributions by the PSCs.

Finally, we have investigated to add the ILAS data to the TOMS data in the whole-day-night regions for TOMS. As a result, we have been successful in making the ILAS-data-added TOMS total ozone maps.

Through the present study, the action of water vapor on the stratospheric chemistry has been confirmed very significant, which agrees with the conclusion from the ASHOE and SPADE projects. Simultaneously, especially in the Polar Regions, as well as the anti-correlation, we have found the proportional correlation and/or no interrelationship between the water vapor and ozone distribution, suggesting other additional undiscussed mechanisms dependent on the spatial and temporal factors.

Acknowledgement

The authors appreciate all the scientists and engineers contributing to the LAS, ILAS, and ILAS-II projects. In particular, the author (A. M.) sincerely thanks the late Professor Tomizo Itoh, who deeply understood and consistently encouraged the LAS project. The science teams of the ILAS and ILAS-II projects have constructed the very high quality ILAS and ILAS-II databases through their researches, including e.g. the validation experiments.

References

[1] Chapman, S., "A Theory of Upper-Atmospheric Ozone," *Memories of Royal Meteorological Society*, III (26). 103-125. 1930.

[2] Bates, D.R, Nicolet, M., "The Photochemistry of Atmospheric Water Vapor," *J. Geophys. Res.*, 55 (3). 301-307. Sep. 1950.

[3] Crutzen, "The Influence of Nitrogen Oxides on the Atmospheric Ozone Content," *Quart. J. Roy. Meteorol. Soc.*, 96 (408). Apr.320-325. 1970.

[4] Molina, M.J, Rowland, F.S, " Stratospheric Sink for Chlorofluoromethanes: Chlorine Atom-Catalysed Destruction of Ozone," *Nature*, 249 (5460). 810-812. Jun.1974.

[5] Steinfeld, J.I, Francisco, J.S, Hase, W.L, *Chemical Kinetics and Dynamics*, Prentice Hall Inc., New Jersey, 1998, 491-492.

[6] Wennberg, P.O, Cohen, R.C, Stimpfle, R.M, Koplow, J.P, Anderson, J.G, Salawitch, R.J, Fahey, D.W, Woodbridge, E.L, Keim, E.R, Gao, R.S, Webster, C.R, May, R.D, Toohey, D.W, Avallone, L.M, Proffitt, M.H, Loewenstein, M., Podolske, J.R, Chan, K.R, Wofsy, S.C, "Removal of Stratospheric O_3 by Radicals: In Situ Measurements of OH, HO_2, NO, NO_2, ClO, and BrO," *Science*, 266 (5184). 398-404. Oct.1994.

[7] Available: http://sage.nasa.gov/. [Accessed Dec. 1, 2014].

[8] Available:http://www.isas.jaxa.jp/j/enterp/missions/ohzora.shtml. [Accessed Dec. 1, 2014].

[9] Available: http://db.cger.nies.go.jp/ilas/index.html. [Accessed Dec. 1, 2014].

[10] Available: http://db.cger.nies.go.jp/ilas2/en/index.html [Accessed Dec. 1, 2014].

[11] " Improved Limb Atmospheric Spectrometer (ILAS)," *J. Geophys. Res. Atmospheres*, Special Section. Oct.2002. Available: http://onlinelibrary.wiley.com/journal/10.1002/(ISSN)2169-8996/specialsection/ILAS1. [Accessed Dec. 1, 2014].

[12] "ILAS-II: The Improved Limb Atmospheric Spectrometer II," *J. Geophys. Res. Atmospheres*, Special Section. Oct.2006. Available: http://onlinelibrary.wiley.com/journal/10.1002/(ISSN)2169-8996/specialsection/ILAS2. [Accessed Dec. 1, 2014].

[13] Matsuzaki, A., Itoh, T., Nakamura, Y., "On Observation of Middle Atmosphere with LAS (Limb-atmospheric Infrared Spectrometer) on Board of Satellite "Ohzora" (EXOS-C)," *J. Meteoro. Soc. Jpn.*, 63 (2). 328-333. Mar.1985.

[14] Matsuzaki, A., "Stratospheri Ozone in Low-Latitude Northern Hemisphere in April 1984," *J. Chem. Soc. Jpn. (Nihon Kagakukaishi, in Japanese), Special Articles on Global and Regional Environment and Chemistry*, 1991 (6). 777-785. 1991.

[15] Matsuzaki, A., Nakamura, Y., Itoh, T., "Rocket Observation of the Rotational Profile of the A-band Absorption Spectrum of Atmospheric Oxygen Molecule," *Annales Geophys.*, 4. 476-480. 1984.

[16] Matsuzaki, A., Nakamura, Y., Itoh, T., " Spectrometers for Rocket, Balloon, and Spacecraft Experiments," in *Multichannel Image Detectors Volume 2*, *ACS Symposium Series*, Vol. 236, Nov.1983, 297-321.

[17] Matsuzaki, A., Nakamura, Y., Itoh, T., " Measurement of Stratospheric Aerosol near Sanriku (39°N, 142°E) in Japan on May 31, 1979," *J. Geophys. Res.*, 88 (C6). 3783-3788. Apr.1983.

[18] Nakajima, H., Suzuki, M., Matsuzaki, A., Ishigaki, T., Waragai, K., Mogi, Y., Kimura, N., Araki, N., Yokota, T., Kanzawa, H., Sugita T., Sasano, Y., "Characteristics and Performance of the Improved Limb Atmospheric Spectrometer (ILAS) in Orbit," *J. Geophys. Res.*, 107 (D24). ILS10-1-ILS10-16. Dec.2002.

[19] Available:http://www.eorc.jaxa.jp/en/hatoyama/satellite/satdata/satellite_config_e.html. [Accessed Dec. 1, 2014].

[20] Matsuzaki, A., Nakamura, Y., Itoh, T., " Rocket - Borne Spectrometer to Measure the Near Infrared Absorption Spectrum of the Upper Atmosphere," *Rev. Sci. Instrum.*, 52 (11). 1685-1689. Nov.1981.

[21] Matsuzaki, A., Nakamura, Y., Itoh, T., "Pyroelectric - vidicon - aided infrared spectrometer for balloon experiments," *Rev. Sci. Instrum.*, 53 (7). 978-983. Jul.1982.

[22] Driscoll, W.G, Vaughan, W., *Handbook of Optics*, McGraw-Hill, New York, 1978.

[23] Shimazaki, T., *Stratospheric Ozone*, 2nd ed., in Japanese, UP Earth Science, The University of Tokyo Publishers, Tokyo, 1989, 44-52.

[24] Available: http://science.nasa.gov/missions/toms/. [Accessed Dec. 1, 2014].

[25] Available: https://archive.org/details/nasa_techdoc_19980235201. [Accessed Dec. 1, 2014].

[26] Available: http://www.metoffice.gov.uk/. [Accessed Dec. 1, 2014].